ISTANBUL TECHNICAL UNIVERSITY ★ GRADUATE SCHOOL

IMPROVEMENT OF ELECTRICAL AND PHOTOCATALYTIC PROPERTIES OF BORON-DOPED ZnO NANORODS AND SYNTHESIS DESIGN OPTIMIZATION BY TAGUCHI APPROACH

M.Sc. THESIS

Eray TABAK

Department of Nanoscience and Nanoengineering

Nanoscience and Nanoengineering Programme

JANUARY 2024

ISTANBUL TECHNICAL UNIVERSITY ★ GRADUATE SCHOOL

IMPROVEMENT OF ELECTRICAL AND PHOTOCATALYTIC PROPERTIES OF BORON-DOPED ZnO NANORODS AND SYNTHESIS DESIGN OPTIMIZATION BY TAGUCHI APPROACH

M.Sc. THESIS

Eray TABAK
(513201031)

Department of Nanoscience and Nanoengineering

Nanoscience and Nanoengineering Programme

Thesis Advisor: Assoc. Prof. Dr. Birgül BENLİ

JANUARY 2024

ISTANBUL TEKNİK ÜNİVERSİTESİ ★ LİSANSÜSTÜ EĞİTİM ENSTİTÜSÜ

BOR-KATKILI ZnO NANORODLARININ ELEKTRİKSEL VE FOTOKATALİTİK ÖZELLİKLERİNİN GELİŞTİRİLMESİ VE TAGUCHI YAKLAŞIMI İLE SENTEZ TASARIMININ OPTİMİZASYONU

YÜKSEK LİSANS TEZİ

Eray TABAK
(513201031)

Nanobilim ve Nanomühendislik Anabilim Dalı

Nanobilim ve Nanomühendislik Programı

Tez Danışmanı: Doç. Dr. Birgül BENLİ

OCAK 2024

Eray TABAK, a M.Sc. student of İTU Graduate School student ID 513201031, successfully defended the thesis/dissertation entitled "IMPROVEMENT OF ELECTRICAL AND PHOTOCATALYTIC PROPERTIES OF BORON-DOPED ZnO NANORODS AND SYNTHESIS DESIGN OPTIMIZATION BY TAGUCHI APPROACH", which he prepared after fulfilling the requirements specified in the associated legislations, before the jury whose signatures are below.

Thesis Advisor :	**Assoc. Prof. Dr. Birgül BENLİ** İstanbul Technical University	.....
Jury Members :	**Prof. Dr. Ömer ŞAHİN** Istanbul Technical University	.....
	Assoc. Prof. Dr. Birgül BENLİ Istanbul Technical University	.....
	Assoc. Prof. Dr. Sadullah ÖZTÜRK Istanbul University-Cerrahpaşa	.....

Date of Submission : 05.01.2024
Date of Defense : 29.01.2024

To my family and my friends,

FOREWORD

As a Bioengineer, I have learned lots of new information during my master's degree programme in Nano Science and Nano Engineering at Istanbul Technical University. First of all, I would like to thank Assoc. Prof. Dr. Birgül BENLİ, who accepted to be my advisor and gave me the opportunity to be a part of the Bee The Surface family, who patiently listened to every suggestion I offered and stood by me by valuing all my ideas.

I would like to express my gratitude to the director of the Institute, Assoc. Prof. Dr. Sadullah ÖZTÜRK, who allowed me to use the laboratory facilities of Istanbul University-Cerrahpaşa Nanotechnology and Biotechnology Institute, supported my thesis from the beginning to the end and helped me in every subject. I would like to thank Şahika Sena BAYAZİT, the director of Istanbul University-Cerrahpaşa Nanotechnology-Biotechnology Institute, who contributed a lot to my thesis and constantly helped us to improve our work. I would like to thank Nevin Nur SELÇUK for helping me with the figures I used in this work. I would like to thank my family who raised me, brought me to this day, supported me from the beginning to the end of every decision I made, and stood by me under all circumstances. I would also like to thank all my friends who constantly motivate me and make me feel that they are with me.

Finally, I would like to thank TUBITAK for the financial support given to the thesis project within the scope of BIDEB - 2210-C Domestic Graduate Scholarship Programme for Priority Areas.

January 2024

Eray TABAK
(Bioengineer)

TABLE OF CONTENTS

Page

ABBREVIATIONS

AC : Alternative Current
Al_2O_3 : Alumina Oxide
B : Boron
Bi_2O_3 : Bismuth Oxide
CuO : Copper Oxide
DC : Direct Current
Fe : Iron
FT-IR : Fourier Transform Infrared Spectroscopy
FWHM : Full Width at Half Maximum
ITO : Indium Tin Oxide
Mg : Magnesium
Mn : Manganese
NiO : Nickel Oxide
O : Oxygen
PET : Polyethylene Terephthalate
SEM : Scanning Electron Microscope
SnO_2 : Tin Oxide
TiO_2 : Titanium Oxide
WHO : World Health Organization
WO_3 : Tungsten Trioxide
XRD : X-Ray Diffaraction
ZnO : Zinc Oxide

SYMBOLS

α	**:** Absorption Coefficient
A	**:** Proportionality Constant
a_0	**:** Lattice parameter
C	**:** Concentration
c_0	**:** Lattice parameter
C_0	**:** Initial concentration
C_t	**:** Concentration at time t
D	**:** Crystal size
d_{hkl}	**:** Space between the planes of the given miller indices h, k, l
E_g	**:** Band Gap Energy
hυ	**:** Photon Energy
I	**:** Current
k	**:** Rate Constant
K	**:** Scherrer Constant
M	**:** Molar
n	**:** Transition mode
nm	**:** Nanometer
t	**:** Time
V	**:** Voltage
β	**:** Full width half maximum in radians
θ	**:** Bragg's Angle
λ	**:** Wavelength
μA	**:** Microamper

LIST OF TABLES

PAGE

LIST OF FIGURES

Page

IMPROVEMENT OF ELECTRICAL AND PHOTOCATALYTIC PROPERTIES OF BORON-DOPED ZnO NANORODS AND SYNTHESIS DESIGN OPTIMIZATION BY TAGUCHI APPROACH

SUMMARY

Today, increasing environmental pollution affects the whole world. One of the most important pollutions among environmental pollution is water pollution. Water pollution seriously threatens living life. With the developing technology, clean water resources are decreasing, and water resources are polluted with industrial and domestic wastes every day. Today, traditional methods are used for water treatment. However, these methods are not able to provide adequate response to water treatment due to low efficiency for small-sized pollution and secondary pollution. Therefore, applications of photocatalysis offer an effective opportunity among advanced oxidative methods; in this study, innovative photocatalyst structures have been developed.

Boron doped ZnO nanorods were successfully synthesised by hydrothermal method and Boron doping has led to enhancements in its photocatalytic and electrical properties. Boron doped ZnO nanorods were grown in two stages. In the first stage, since dipole forces will be effective for growth, the thin film called seed layer layer on the glass surface was coated with the surface spin coating method. Then, with zinc nitrate dehydrate and hexamethylenetetetraamine added in equal molar amounts, nanorods were grown on the glass with seed layer at 90 °C for 3 hours. X-ray diffaraction (XRD), UV-Vis spectrometer, FT-IR, DC electrical analysis (I-V), AC electrical analysis, characterisation by Scanning electron microscopy (SEM) and photocatalytic analysis by UV-A 366 nm light were also performed. Then, Taguchi experimental design method was used to determine the best conditions for selected parameters such as pH, pollutant concentration, time, additive amount and to calculate the effects between each other. The XRD results indicate that boron has successfully integrated into the structure. Also, pure and boron doped ZnO nanorods grew in wurtzite structure and the crystal sizes were confirmed by SEM images. As a result of FT-IR analysis, it was shown that the peak belonging to B-O, B-O-B bonds increased with the increase in doping. It was proved that the band gap intervals calculated as a result of UV-Vis spectrometry analysis decreased with boron doping. Electrical analyses showed that the electrical conductivity increased with increasing boron doping.

As a result of all these analyses, electrical conductivity increased from 0.03 μA for pure ZnO to 1.9 μA for 10% boron doped ZnO. With the increase in surface defect, the band gap decreased with the increase in conductivity, boron doping was proven to increase the number of electrons and it was thought that their photocatalytic activity should increase. As a result of photocatalytic tests, it was shown that the efficiency

increased with boron doping. When we compare the numerical values of the rate constants, under the same conditions, the 1% B doped sample has a 94% higher rate than the pure ZnO sample for pH 4. For pH 7, the 3% B-doped sample has a 36% higher rate than pure ZnO, and finally for pH 10, the 7% B-doped sample has a 194% higher rate constant. Moreover, the effect of pH was discussed. It was observed that boron doped ZnO nanorods had better photocatalytic efficiency for each pH range and concentration. As a result of the calculated rate constants, 3% boron doping for $2x10^{-6}$ M concentration, pH 7 showed the best result with a rate constant value of 0.00856 min^{-1}. Finally, optimized parameters for pH 4, concentration $2x10^{-6}$ M, time 90 min and doping amount 7% were determined by Taguchi method. As a result of ANOVA analysis, the model was proved to be 85% fit.

BOR-KATKILI ZnO NANORODLARININ ELEKTRİKSEL VE FOTOKATALİTİK ÖZELLİKLERİNİN GELİŞTİRİLMESİ VE TAGUCHI YAKLAŞIMI İLE SENTEZ TASARIMININ OPTİMİZASYONU

ÖZET

Günümüzde artan çevre kirliliği tüm dünyayı etkilemektedir. Çevre kirliliği sebebiyle, Dünya Sağlık Örgütü verilerine göre her yıl yaklaşık 9 milyon insan ölümüne sabep olduğu düşünülmektedir. Çevre kirliliği sebepleri arasında endüstrinin filtre kullanmadan zararlı kimyasalları atmosfere salması, ikincil kirliliklerin toprağa karıştırılması, elektronik malzemeler aracılığı ile toprağa ağır metallerin karışması, esele ve endüstriyel atıklar ile tonlarca krili suyun temiz su kaynaklarına karıştırılması sayılabilir. Çevre kirliliği bu sebeple hava, su, toprak olmak üzere üç ana başlıkta toplanmaktadır. Çevre kirliliği arasında en önemli kirliliklerden bir tanesi su kirliliğidir. Su kirliliği canlı yaşımını ciddi şekilde tehdit etmektedir. Gelişen teknoloji ile birlikte temiz su kaynağı azalmakta ve her geçen gün endüstri ve evsel atıklarla beraber su kaynakları kirletilmektedir. Bu sebeple milyonlarca insan kirli su kaynaklarından su tüketmektedir. Bu sorun pek çok canlının hayatını tehlikeye atmaktadır. Günümüzde su artımı için geleneksel yöntemler kullanılmaktadır. Ancak bu yöntemlerin yüksek maliyetli olması, küçük boyuttaki kirlilikler için düşük verimde olması, ikincil kirlilik yaratması yüzünden su arıtımına yeterli cevabı verememektedirler. Bu sebeple özellikle nanoteknolojinin gelişmesiyle çeşitli yeşil artıma yöntemleri ortaya çıkmıştır ve bir çok bilim insanı bu yöntemleri geleneksel sistmelere entegre ederek yüksek verimli, düşük maliyetli su arıtım sistemleri elde etmeye çalışmaktadırlar. İleri oksidatif yöntemlerinden bir olan fotokataliz yöntemi sadece ışık ve ışığı absorbe eden yüzeylerin yardımı ile su arıtımı sağlayan yöntemlerden bir tanesidir. Düşük maliyetli olması, ikincil kirlilik yaratmaması ve kolay üretilebilir olması sebebiyle cazip yöntemlerden birisidir. Bu sebeple bu çalışmada ileri oksidatif yöntemlerinden biri olan fotokatalitik yöntem üzerinde durularak, yenilikçi ve yüksek verimli fotokatalizörler geliştirilmesi amaçlanmaktadır.

ZnO, II-IV grubu bir yarı iletkendir ve oda sıcaklığında geniş band enerjisine ve yüksek eksiton enerjisine sahip olması, biyouyumli ve biyo-güvenli olması, yüksek kimyasal kararlılığa sahip ve radyasyona karşı dirençli olması, düşük maliyetli olması onu uygun bir fotokatalizör adayı yapmaktadır. Ancak tüm özelliklerine rağmen hızlı rekombinasyon, geniş band gap enerjisi, fotokorozyon gibi fotokatalitik verimi düşüren ksıtlayıcı faktörelere sahiptirler.

ZnO'nun fotokatalitik özelliklerini geliştirmek için yaygın olarak morfoloji kontrolü, metal katkılama, non metal katkılama, yarı-metal katkılama, komposit yapı oluşturma

gibi pek çok yöntem denenmiştir. ZnO 1-2-3 boyutlu nano yapılarda bulunmaktadır. Seçilen sentez yöntemine, ortam faktörlerine bağlı olarak oluşan yapılar değişmektedir. Bilinen gerçek şu ki 1-D yapılar en yüksek yüzey alanına sahiptir. Yüzey alanın artması, fotokatalitik verimin artması ile doğrudan orantılıdır. Bor elementi, düşük yarıçapa sahip olması, yüksek elektronegatifliğe sahip olması, stabilitesinin yüksek olması ve asit direncinin bulunması gibi özellikleri sebebiyle ZnO'da bulunun kısıtlayıcı faktörlerin üstesinden gelineceği düşünülmektedir.

Bu çalışmada sentez yöntemi olarak kolay ve uygulanabiliri yöntem olan hidrotermal yöntem kullanılmıştır. Hidrotermal yöntem ile Bor katkılı ZnO nanorodların başarı ile sentezi gerçekleşmiş ve fotokatalitik, elektriksel özelliklerinin geliştirilmesi sağlanmıştır. Bor katkılı ZnO nanorodlar iki aşamada cam yüzeyler üzerinde büyütülmüştür. İlk aşamada büyüme için dipol kuvvetlerin etkisi olacağından cam yüzey üzerinde çekirdekleyici tabakası (seed layer tabakası) denen ince film yüzey, spin coating yöntemi ile kaplanmıştır. Ardından eşit molarda eklenen çinko nitrat dekahidrat ve hekzametilentetraamin ile 90 °C'de 3 saat ağzı sıkıca kapalı bir cam şişe içerisinde fırında, çekirdekleyici tabakaya sahip camlar üzerinde nanorod büyümesi sağlanmıştır. Hekzametilentetraamin ZnO oluşması için gereken hidroksil iyonlarını sağamak amacıyla ve pH dengelemek amacıyla kullanılmıştır. Bu çalışmada bor katkısı, büyüme aşamasında gerçekleştirilmiştir. Bor katkısı için kullanılan malzeme borik asittir. Hidrotermal büyüme çözeltisi için eşit molarda (0,01 M), Zinc nitrate hexahydrate ($Zn(NO_3)2\cdot 6H_2O$) ve Hexamethylenetetramine ($C_6H_{12}N_4$) 80 ml ultra saf su içerisinde oda sıcaklığında 1 saat boyunca karıştırılırken yanda borik asit ultra saf su içerisinde karıştırılmaya bırakılır. Çözünen borik asit, hidrotermal çözeltisine kütlece %1,3,5,7,10 olacak şekilde eklenmiştir.Fırından çıkarılan camlar su ile yıkanarak oda sıcaklığında kurumaya bırakılmıştır. X-ray Difraksiyon (XRD), UV-Vis spektrometre, Fourier Dönüşümü Kızılötesi Spektroskopisi (FT-IR), DC elektriksel analiz (I-V), AC elektriksel ölçümler, Taramalı elektron mikroskobu (SEM) ile yüzey görüntülemesi yapılmıştır.

Fotokatalitik testler kapalı ortamda 366 nm'de UV-A ışık altında yapıldı. Kirletici olarak Metilen Mavisi kullanılmıştır. Metilen Mavisi 3 farklı konsantrasyonda hazırlandı. Sırasıyla hazırlanan konsantrasyonlar $2x10^{-6}$, $1x10^{-5}$ M, $5x10^{-5}$ M. Seyreltik HCl ve NaOH kullanılarak pH ayarlaması yapıldı. Her bir konsantrasyon 4, 7 ve 10 pH aralığında hazırlandı. PH aralığı, pH metre ile kontrol edilerek yapıldı. Ardından hazırlanan Metilen Mavisi konsantrasyonları, 3ml olacak şekilde, önceden temizlenmiş quvars camlara aktarıldı. Öncelikle ışığın MB degredasyonu üzerindeki etkisini ölçmek için quvars içerisinde Metilen Mavisi konsantrasyonları 90 dakika ışıklı ortamda tutuldu. UV-Vis spektrometre kullanılarak absorbans değişimi ile konsantrasyon arasında ilişki kurularak konsantrasyon değişimi takibi yapıldı. 90 dakika ışık altında bekletilen Metilen Mavisi konsantrasyonlarında dikkate değer bir degredasyon gerçekleşmedi. Fotokatalitik deneyler için quvarsların içerisine yüzeyi B katkılı ve katkısız ZnO kaplı 1x2 cm camlar dikey olarak eklendi. Adsorpsiyon-deadsorpsiyon dengesinin gerçekleşmesi için 40 dk karanlık ortamda bekletildi. Ardından numuneler toplam 90 dk olacak şekilde ışık altında bırakılarak fotodegredasyon gerçekleşmesi beklenmiştir.Ardından minimum deney sayısı ile pH, kirletici konsantrasyonu, zaman, katkı miktarı faktörleri arasında en iyi koşulların belirlenmesi, birbiri arasındaki etkilerin hesaplanması için Taguchi yaklaşımıyla deneysel tasarım yapılarak optimum değerler elde edilmiştir. Taguchi yaklaşımı kaliteyi arttırmak ve maliyeti düşürmek amacıyla ortaya çıkmıştır. Bu yaklaşım, deney

parametrelerini optimize etmek için kullanılan kolay ve başarılı bir tekniktir. Taguchi yaklaşımı, tüm süreç parametrelerini az sayıda deney yapılarak araştırmak için özel bir ortogonal dizi tasarımı kullanılır. Klasik deneysel tasarım yöntemlerine göre avantajlar sunar. Ayrıca bu yaklaşım, sonuç değişkeninin varyasyonunu azaltır ve optimum proses koşullarını bulmanın en iyi yolunu gösterir. Deney tasarımında optimum proses koşullarını belirlemenin ve verimliliği artırmanın en iyi ve en ekonomik yoludur.

Elde edilen XRD sonuçlarıyla saf ve bor katkılı ZnO nanorodlarımızın wurtzite yapıda büyüdüğü gösterilmiştir. Büyümenin tek yönelimde olduğu ve sonrasında artan katkı miktarı ile yeni bir pikin oluştuğu gözlenmiştir. Bu pikin bor katkısı ile değişen polarlık sonucu olduğu düşünülmektedir. Ayrıca elde edilen sonuçlar ile kristal boyutları hesaplanmış ve kristal boyutları SEM ile doğrulanmıştır. FT-IR analizi sonucunda B-O, B-O-B bağlarına ait pikin katkının artmasıyla arttığı gösterilmiştir. UV-Vis spektrometre analizi sonucunda hesaplanan band gap aralıklarının, bor katkısı ile birlikte düştüğü kanıtlanmıştır. Elektriksel analizler sonucundan ise bor katkısının artmasıyla, elektriksel iletkenliğin arttığı gösterilmiştir. Bor katkısının artması yarımetal olarak davranan ZnO'nun metalik forma geçişini sağladığı gözlemlenmiştir. Bu durumda daha fazla elektronun sisteme girdiğini ve enerji seviyeleri arasında yeni tuzak seviyeleri oluşturduğu söylenebilir. Bu saye de hem ZnO tarafından kaybedilen elektronların geri kazanılması, hemde daha fazla elektronun tutulması sağlanmıştır diyebiliriz. Bunun sonucunda da doğal olarak band boşluğu enerjisinin düşmesini ve iletkendiğin artmasını beklemekteyiz. Nitekim AC ve DC analizler sonucunda iletkenliğin bor katkısı ile beraber arttığı gösterilmiştir.
Tüm bu analizler sonucunda elektriksel iletkenlik saf ZnO için 0.03 μA iken %10 bor katkılı ZnO için 1.9 μA yükselmiştir. Bor minerali ZnO oluşumu esnasında oksijenlerin kristal yapıdan almış olduğu, yoksunluk hissedilen elektronları ZnO kristal yapısına geri kazandırarak iletkenlik davranış tipini yarıiletkenlik formundan katkı oranına bağlı olacak şekilde metalik forma doğru değiştirmektedir. Ancak unutulmamalı ki, sıcaklık artışı ile metallerin elektriksel iletkenlikleri artmak yerine azalış göstermektedir. Bizim burada ki yorumumuz, bor katkısının ZnO'nun kristal yapısına elektron vererek elektriksel iletkenlik davranışının değişmesidir. Fotokatalitik testler sonucunda da bor katkısı ile verimin arttığı, yüksek bor katkısı oranında ise dikey yönlenmelerin ve rod uzunluklarının azalmasıyla verimin düştüğü görülmüştür. Ardında Ph'ın fotokatalitik verim üzerine etkisi tartışılmış. Her pH aralığı ve konsantrasyon için bor katkılı ZnO nanorodların daha iyi fotokatalitik verime sahip olduğu görülmüştür. Hesaplanan hız sabitleri sonucunda da $2x10^{-6}$ M konsantrasyon, pH 7 için %3 bor katkısının 0,00856 min^{-1} hız sabiti değeri ile en iyi sonucu gösterilmiştir. Hız sabitlerinin sayısal değerlerini karşılaştırdığımızda ise aynı koşullar altında %1 B katkılı numune, pH 4 için saf ZnO numunesinden %94 daha yüksek orana sahiptir. pH 7 için %3 B katkılı numune, Saf ZnO'dan %36 daha yüksek oran ve son olarak pH 10 için %7 B katkılı numune %194 daha yüksek hız sabitine sahiptir.

Son olarak Taguchi yaklaşımında dört farklı faktör seçilerek bu faktörlerin birbirlerine ve degredasyon oranına etkisi incenlemiştir. Bu faktörler pH, kirletici konsantrasyonu, katkı miktarı ve zamandır. Seçilen deneysel faktörler göz önüne alındığında fotokatalitik deneylerin optimizasyonu, Taguchi yöntemi ile pH 4, konsantrasyon $2x10^{-6}$ M, süre 90 dk ve dop miktarı %7 olarak belirlenmiştir. ANOVA analizi sonucunda modelin %85 uyumlu olduğu kanıtlanmıştır. Taguchi yaklaşımı ile ortaya çıkan bu değerlendirmeler bize en etkili faktörün zaman ve konsantrasyon olduğunu,

sonrasında katkı miktarının geldiğini göstermektedir. PH aralığı bu yaklaşım sonuçlarına göre çok fazla etkili gözükmemektedir. Ancak sentezlenen yeni fotokatalizörümüzün düşük pH aralıklarında çalışabiliyo olması fotostabilitenin arttığını göstermektedir. Tüm bunların ışığında elde edilen bor katkılı ZnO nanorodların özelliklerinin geliştirilmesi başarıyla gerçekleştirilmiştir. Bor katkılı ZnO nanorodları, gelişmiş sistemlere entegre ederek su arıtımı ve hava arıtımı gibi alanlarda kullanabiliriz. Bu sayede enerji ve zamandan tasarruf edebiliriz. Ayrıca gelen elektriksel iletkenlik sonuçları da bize sensör ve elektronik alanları için de uygun olduğunu göstermektedir. Hidrojen depolama, sensörler, akıllı devreler, temiz arıtım için potansiyeli bulunmaktadır.

1. INTRODUCTION

1.1 Purpose of Thesis

Today, nanotechnology has been integrated into our lives in many areas. The striking changes in the properties of nanosized materials have pushed scientists in every field to study, discover, learn and develop. With the development of nanotechnology, an issue that is perhaps not valued enough in the world has started to rise in a negative sense. This issue is environmental pollution. But we should not forget that the solution to pollution lies in nanotechnology and the methods to be developed.

This thesis is a search for a solution to reduce pollution, at least to some extent. Our aim is to focus primarily on water pollution and ensure that pollution is eliminated without creating secondary pollution. While doing this process, we aim to use minimum energy. In this study, it is aimed to eliminate the pollution in water by photocatalysis method, which is an advanced oxidative process method. It is aimed to improve the negative aspects of ZnO, a metal oxide photocatalyst, with the addition of Boron in order to achieve photocatalytic removal in the presence of light. In this way, it is among our goals to increase the added value of Boron mineral, which is considered the national mineral of our country, by integrating it into nanotechnology.

In this study, it is aimed to synthesize boron-doped ZnO nanorods using the hydrothermal method, then characterization them, improve their electrical and photocatalytic properties, and determine the best conditions and contribution within the framework of the factors determined by doing minimum experiments with the Taguchi method.

1.2 Literature Review

In 1959, Richard Feynmen invited a new facet of physics by saying, "There is plenty of room at the bottom." [1]. This is how nanotechnology started to enter our lives. Nanotechnology is not a branch of technology that only covers materials.

Nanotechnology covers controllable materials, devices and all systems integrated with them between 1-100 nm. With the introduction of nanotechnology into our lives, systems, devices and materials that we still have difficulty keeping up with are being developed and working continuously to make human life easier. Although it provides us advantages in every field, it also has some disadvantages. Especially with the development of technology and the development of industry, pollution that threatens life has emerged. Air, water and soil pollution are among the leading problems. This pollution, which continues to increase with the development of technology, will also be eliminated with technology. In this section, water pollution will be discussed under environmental pollution, followed by the emerging methods to remove pollution. The impact of nanotechnology on these methods and the methods developed with nanotechnology will be discussed

1.2.1 Environmental pollution

Nowadays, one of the biggest problems faced by the world is environmental pollution. Every behaviour that causes deterioration of the natural environment is considered as pollution [2]. Increasing environmental pollution has led to the emergence of many diseases and started to threaten human life. Last years, premature deaths due to environmental pollution are thought to be close to 9 million [3]. Thus, pollution has become closely related to human life and the future of living. The main effects of pollution include factors such as climate change, population growth, developing industry, chemicals, agriculture, urbanisation, fossil fuel use. Low and middle income countries create more pollution than developed countries. The reason for this can be listed as using more fossil fuels, lack of deterrent laws against environmental pollution [4]. In addition, the movement of electronic and electrical equipment transferred from developed countries to developing countries results in the mixing of toxic metals into air, water and soil [5]. Environmental pollution is a world problem and no country is blameless. Especially with the increase in industry, a lot of wastewater is mixed into clean water sources, and many harmful chemicals are released into the soil and air. Therefore, environmental pollution appears under three main headings. These are air pollution, soil pollution and water pollution. Environmental pollution shows in Figure 1.1. We will focus on water pollution.

Figure 1.1: Types of environmental pollution and remediation method.

1.2.2 Water pollution

Water pollution occurs when undesirable substances mix into water, change the quality of water, and harm the environment and human health [6]. Water is a very important natural resource for drinking and other vital activities in nature. Water is the most basic compound for the human body. Therefore, water pollution seriously affects human health and the health of other living things [7]. Access to safe drinking water is very important. According to World Health Organization (WHO) data, approximately 2 billion people consume water from contaminated water sources. Drinking water in different countries of the world does not comply with WHO standards [8]. For this reason, clean natural water supply is very important for humanity. There are many causes of water pollution, both natural and man-made. If we give an example of natural pollution, we can give an example of ores that make groundwater resources rich in toxic metals [9]. Apart from these, we cannot pass without mentioning the pollution caused by developing technology and human activities. Domestic wastes, industrialisation, pesticides, fertilisers, synthetic and organic dyes, plastics, urbanisation, poor management are among the main causes of water pollution. Sectors such as domestic waste, textile, pesticide, paper are the leading sectors in wastewater production. These wastes are discharged into rivers almost untreated [10]. About 70%

of the pollution is caused by domestic wastes and sewage, while 25% is caused by industry and is more harmful [11]. To give an example, synthetic and organic paints are used in many fields. Approximately $7x10^7$ tonnes of dyes are produced annually [12]. According to the research of Jin et al. among these dyes, it is estimated that approximately 280.000 tonnes of dyes used in the textile industry are mixed with wastewater [13]. In response to the rapid increase in water pollution, many water treatment methods have been tried to be developed. In the next section, the methods developed and being developed will be discussed.

1.2.3 Water treatment method

Over time, a variety of methods have been developed to address the issue of water pollution. Typically categorized as conventional approaches, physicochemical methods are employed in water treatment. Commonly utilized techniques encompass coagulation/agglomeration, aeration screening, filtration, straining, sedimentation, disinfection, and fluoridation. Additionally, specialized treatment systems involve ion exchange, pre-disinfection, electrodialysis, activated carbon adsorption, pre-precipitation, reverse osmosis, and chlorination/fluorination. [14]. These methods are implemented either independently or in conjunction. However, traditional methodologies exhibit certain drawbacks in water treatment, including high costs, the likelihood of producing secondary pollution, lengthy processing times, and susceptibility to external influences. [15]. For instance, wastewater discharge can easily spread in the environment, posing risks to human health. Coagulation and flocculation processes can generate secondary effluents by aggregating microflocs into visible colloids or pin flocs, potentially leading to the production of other hazardous substances [16]. Biological and ecological methods necessitate prolonged procedures, and their efficiency can be impacted by external factors like weather conditions [17]. In order to minimise these problems, the need for new methods has arisen. New methods are being developed by integrating nanotechnology and nanomaterials into water treatment to minimise the problems arising with traditional methods [15]. Advanced nanotechnology and traditional methods can combine to provide solutions to control the damage caused by water pollution.

1.2.4 Nanotechnology and water treatment

Nanotechnology encompasses applications at the nanoscale, involving the control or manipulation of matter at the atomic or molecular level, typically ranging from 1 to 100 nanometres [18]. It spans the production and modification of physical, chemical, and biological systems, nanomaterials, and the integration of nanostructures into larger systems, spanning from atomic to submicron sizes. [19]. At the nanostructural level, materials undergo significant alterations in their properties, including physical, electrical, chemical, optical, and biological attributes. [20]. Since the 20th century, nanotechnology has been embedded in our lives, enabling its integration into larger systems owing to its manageable physical, chemical, and optical characteristics. Revolutionary advancements have been offered by smart materials to address a multitude of contemporary environmental, medical, and industrial challenges, such as nano-manufacturing, electronics, drug delivery, energy and water treatment, biotechnology, information technology, and national security [15].

Nanotechnology employs nanometre-sized materials, devices, and systems for water pollution remediation and water quality management [21]. The distinctive and diverse properties of nanomaterials—such as their expansive specific surface area, high reactivity, multifunctionality, size-dependent characteristics, and specificity towards particular contaminants—render them exceptionally well-suited for water purification and wastewater treatment [22]. Leveraging these nanomaterial traits has led to the development of low-energy, environmentally friendly methods like nanofiltration, ion exchange, adsorption, and advanced oxidation processes (photocatalaysis). Nanotechnology holds the promise of addressing concerns stemming from the deleterious by-products of conventional water treatment methods. Moreover, the advanced attributes of nanomaterials offer solutions to mitigate water quality degradation during distribution [23]. Additionally, energy-efficient methodologies developed through nanotechnology can serve as an alternative water source during catastrophic events [24].

1.2.5 Photocatalysis

Photocatalysis is one of the advanced oxidation processes. Photocatalysis is a combination of photochemistry and catalysis [25]. Photocatalysis basically involves the acceleration of chemical reactions in the presence of light and catalyst [26]. The

idea of catalysing a chemical process with the help of a compound in the presence of light was introduced by Plotnikow in 1910 and Landau in 1913 [27]. After the 1940s, photocatalytic properties of oxides, semiconductor-containing dyes and textiles were discovered and investigated in order to extend their lifetime Since the late 1970s, photocatalytic processes have been investigated as effective tools for solving environmental problems thanks to studies such as the photoassisted electrodeposition of water on titanium dioxide electrodes by Fujishima and Honda [28] and the photocatalysed reduction of carbon dioxide on irradiated semiconductors by Inoue et al [29]. Today, photocatalysis is used for many purposes such as anti-scaling, air purification, energy storage, hydrogen production, deodorisation, sterilisation, self-cleaning, wastewater treatment. [30] .

Photocatalysis occurs with light and light-retaining surfaces called photocatalysts, which are generally made of semiconductor materials [31]. It is divided into two as homogeneous and heterogeneous photocatalysis. Homogeneous photocatalysis is a system in which reactants and photocatalysts are in the same phase. The best examples for these are ozone systems and fenton systems. Heterogeneous photocatalysis is a system in which reactants and photocatalysts are in different phases. Light absorbing semiconductors are generally used as photocatalysts [32]. In this type of photocatalysis, firstly light falls on the surface of the photocatalyst and is absorbed. The absorbed photons excite the electrons on the surface, allowing the electrons in the valence band to pass to the conduction band. The energy required for the electrons to pass from the valence band to the conduction band is called band gap energy or band gap energy is known as the energy difference between the conduction band and the valence band. This leads to the formation of electrons in the conduction band and holes in the valence band. This is called an electron-hole pair. At this time, hydroxyl radical and oxygen anion radicals are formed by reduction-oxidation reactions. These radicals can react irregularly and rapidly. In this way, they react with organic compounds and ensure their elimination [33-34]. In order for all these processes to take place, photocatalysts must have the ability to absorb light, form electron-hole pairs, and form charge carriers when excited with the required amount of energy. For this reason, metal oxides, metal sulphides, metal organic frameworks, polymeric materials are used as photocatalysts due to their various properties [35].

1.2.6 Metal oxides

Metal oxides, characterized by a tightly packed structure, form through the bonding of metal ions and oxide ions, establishing coordination bonds [36] These oxides exhibit distinct physical and chemical properties. In their nanostructured form, owing to their unique attributes, they find diverse applications such as heavy metal removal, sensing toxic gases, textile coating for wearable electronic devices, biomedical uses, and the photocatalytic degradation of organic pollutants [37]. The surface area of metal oxides increases significantly at the nanoscale, enhancing their reactivity compared to other crystals [38]. Nanomaterials based on metal oxides possess adjustable structural, crystalline, and surface characteristics, operating as semiconductors with wide band gaps [39]. In various energy and environmental domains, sustainable photocatalytic materials are imperative to be abundant, cost-effective, and environmentally benign. Metal oxides possess these requisite traits, positioning them as promising photocatalyst [40] s. Photocatalytic systems make use of metal oxide species like titanium dioxide (TiO_2), zinc oxide (ZnO), copper oxide (CuO) [41], tin oxide (SnO_2) [42], bismuth oxide (Bi_2O_3) [43], tungsten trioxide (WO_3) [44], alumina oxide (Al_2O_3), nickel oxide (NiO) [45], iron-based oxides. Notably, TiO_2 and ZnO emerge as the most extensively utilized photocatalysts among these [46].

1.2.7 Zinc oxide

Nanostructured ZnO has long attracted attention due to its superior properties in electronics, optics and photonics [47]. ZnO is a group II-IV, n-type semiconductor [48]. Since it has a wide band gap energy and high exciton energy at room temperature, it is actively used in optical and photonic, sensor applications. At the same time, it does not show any toxic properties due to its biocompatibility and biosafety. ZnO has high chemical stability and its resistance to radiation makes it one step ahead of other metal oxides. ZnO has a large number of active surface defects, resulting in high surface reactivity [49-50]. ZnO has three types of crystal structures. These crystal structures are rocksalt, zinc blende and wurtzite structures. Rocksalt structure is rare because it is formed in high pressure conditions. The most stable and most common structure is the hexagonal wurtzite structure [51]. The crystal nature of ZnO can be indexed to the known structures of hexagonal ZnO with a = 0.32498 nm, b = 0.32498 nm and c = 5.2066 nm (JCPS card no. 36-1451) [52]. The c/a ratio of about 1.60 is

close to the ideal value of c/a = 1.633 for a hexagonal cell [53]. Cristal structures are shown in Figure 1.2. O^{2-} and Zn^{2+} form a tetrahedral unit and the whole structure lacks central symmetry in Figure 1.2c. This causes it to exhibit piezoelectronic properties when interacting with an electromechanical coupling [54]. Table 1.1 shows the properties of ZnO. ZnO is a very suitable candidate for photocatalyst due to its high stability, high reactivity, large surface area, large band gap energy, surface defects, modifiable structures, cheap and accessible. ZnO can be found in one-dimensional structures such as, nanowire, nanorod, nanobelt [55], nanoring [56], nanoneedle [57] two-dimensional structures such as nanosheet, nanopellet [58] and three-dimensional structures such as flower, snowflake [59]. There are various synthesis and growth methods to obtain these structures.

Table 1.1: Properties of wurtzite ZnO [60].

Lattice Parameters At 300 K	
Properties	Value
a_0	0.324 95 nm
c_0	0.520 69 nm
a_0/ c_0	1.602 (ideal hexagonal structure shows 1.633)
μ	0.345
Density	5.606 g cm^{-3}
Stable Phase At 300 K	Wurtzite
Melting Point	1975 ℃
Thermal Conductivity	0.6, 1–1.2
Linear Expansion Coefficient (/C)	a_0:6.5×10^{-6} c_0:3.0×10^{-6}
Static Dielectric Constant	8.656
Refractive İndex	2.008, 2.029
Energy Gap	3.37 eV, direct
Intrinsic Carrier Concentration	<106 cm^{-3}
Exciton Binding Energy	60 meV
Electron Effective Mass	0.24
Electron Hall Mobility At 300 K For Low N-Type Conductivity	200 cm^2 V^{-1} s^{-1}
Hole Effective Mass	0.59
Hole Hall Mobility At 300 K For Low P-Type Conductivity	5–50 cm^2 V^{-1} s^{-1}

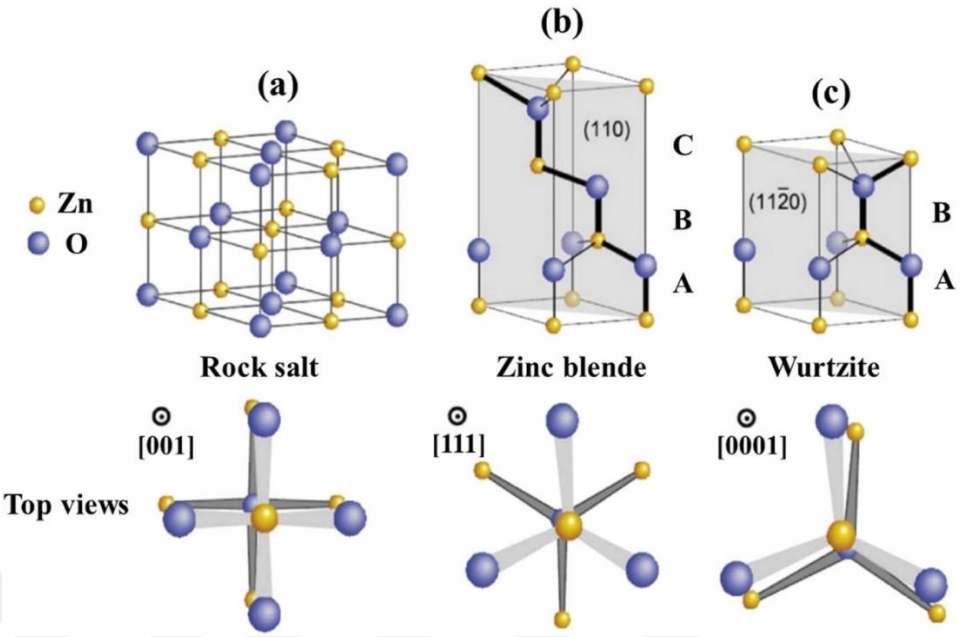

Figure 1.2: Different Crystal Structure of ZnO [61].

1.2.7.1 ZnO photocatalytic mechanism

The photocatalytic mechanism of ZnO will be explained by equations and Figure 1.3. When ZnO is excited by a photon with an energy equal to or greater than the band gap energy, electrons in the valence band rise to the conduction band and a hole is formed in the valence band (Eq 1.1). The generated electron-hole pairs then move to the ZnO surface and participate in reduction-oxidation reactions. They are captured by electron-hole scavengers to prevent recombination. Oxygen and hydroperoxyl radicals play an important role here as electron scavengers to prevent recombination. In the absence of an electron scavenger, the electron-hole pair combines and generates heat. In the conduction band, electrons interact with oxygen to produce superoxide radical anions. Then this reaction continues until hydrogen peroxide is formed and hydroxyl radical is formed by reacting with superoxide radicals (Eq 1.2-1.5). Hydrogen peroxide can also react with electrons to form hydroxyl radicals (Eq 1.6-1.7). Meanwhile, h^+ in the valence band interacts with water and hydroxyl ions to form hydroxyl radicals (Eq 1.8-1.9). The hydroxyl radicals produced enable the elimination of pollutants to harmless compounds such as water and carbon dioxide because hydroxyl radicals act as a strong oxidising agent (Eq 1.10). The photocatalytic mechanism is described in Figure 1.3 [51, 61- 62].

$$ZnO + h\upsilon \rightarrow e^- + h^+ \quad (1.1)$$

$$\bullet O_2 + e^- \rightarrow \bullet O_2^- \quad (1.2)$$

$$\bullet O_2^- + H^+ \rightarrow \bullet HO_2 \quad (1.3)$$

$$\bullet HO_2 + \bullet HO_2 \rightarrow H_2O_2 + O_2 \quad (1.4)$$

$$H_2O_2 + \bullet O_2^- \rightarrow \bullet OH + OH^- + O_2 \quad (1.5)$$

$$H_2O_2 + h\upsilon \rightarrow 2 \bullet OH \quad (1.6)$$

$$H_2O_2 + e^- \rightarrow \bullet OH + OH^- \quad (1.7)$$

$$H_2O_2 + h^+ \rightarrow \bullet OH + H^+ \quad (1.8)$$

$$OH^- + h^+ \rightarrow \bullet OH \quad (1.9)$$

$$\bullet OH + pollutant \rightarrow intermediates \rightarrow CO_2 + H_2O \quad (1.10)$$

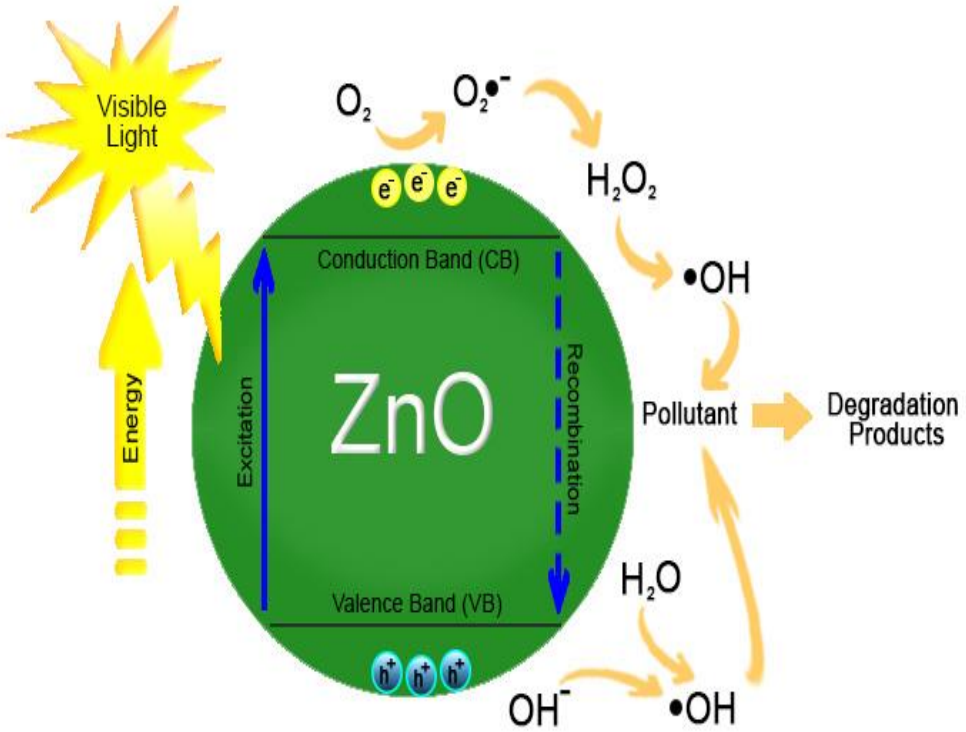

Figure 1.3: Mechanism of Photocatalysis on ZnO surface.

1.2.7.2 ZnO synthesis method

There are two main approaches to synthesise nanostructures. These are top down and bottom up. Top down refers to the cutting of large parts down to nanostructure. Bottom up, on the other hand, nanostructures are obtained from smaller particles such as atoms or molecules [63]. The method chosen for ZnO production changes the morphological and structural properties. Many methods have been developed and used to obtain ZnO nanostructures. Over time, certain methods have come to the fore. Among the reasons for coming to the forefront are low cost, controllability, accessibility and high quality. In this chapter, sol-gel method, hydrothermal method, thermal decomposition, green synthesis, microwave-assisted combustion, co-precipitation are discussed and shown in Table 1.2.

1.2.7.2.1 Sol-Gel method

Sol-Gel method is one of the most widely used wet chemistry methods to produce nanostructures of different materials. It provides large surface area and stability to the nanostructures formed. The method is carried out in two stages. Firstly, a colloidal solution called sol is obtained by hydrolysis of precursor materials. Then, liquid sols are converted into solid gels by polymerisation. Temperature can be used to condense the material [64].

Benhebal et al. [65] obtained ZnO nanoparticles with zinc acetate and oxalic acid precursor materials using sol-gel method. They showed that the size of these particles was approximately 30 nm. Then, they tested phenol removal under light to see the photocatalytic properties of the nanoparticles they obtained. According to their study, approximately 60% removal was achieved in 120 minutes.

Hasnidawani et al. [66] obtained ZnO nanostructures by sol-gel method using zinc acetate and ethanol. Their aim was to obtain a controllable, modifiable ZnO structure using sol-gel method. As a result of their experiment, they successfully obtained ZnO nanoparticles. The size of the nanoparticles they obtained is approximately 82 nm.

1.2.7.2.2 Thermal decomposition

Thermal decomposition is the chemical decomposition of the parent compound by temperature. Thermal decomposition, which is a low-cost method, is an effective and

easy method used to obtain metal oxide nanoparticles. The desired nanostructures can be synthesised without any catalyst, surfactant, organic or toxic solvent [63].

Saravanan et al. [67] obtained ZnO from zinc acetate at different temperatures using thermal decomposition method. At 950 °C, the ZnO nanoparticles obtained were tested photocatalytically in a liquid in a closed environment. They used methylene blue and methyl orange as pollutants. As a result of the experiment, they obtained a degradation of approximately 97% and 80%.

1.2.7.2.3 Hydrothermal method

Hydrothermal method is one of the most frequently used methods. It takes place under high pressure and temperature. It is used to produce small-sized materials. Single crystalline metal nanostructures are obtained from the liquid phase. It is a low-cost, highly efficient, accessible method. With this method, no organic solvent or extra processing is needed. Desired properties can be obtained by changing temperature and pressure [68].

Kumaresan et al. [69] obtained ZnO nanoparticles by hydrothermal method using zinc chloride. They examined the structures to be formed by changing the pH of the medium during synthesis and then tested their photocatalytic properties. As a result of the study, they showed that the pH of the solution had no effect on the optical band gap. Rhodamine B was used as pollutant. As a result of the experiment, approximately 94% removal was shown.

Agarwal et al. [70], successfully synthesised ZnO nanorod/flower structures on zinc acetate precursor using hydrothermal method. Their aim was to test their gas measurement properties. As a result of their studies, they proved that nanoflower structures are more sensitive to NO_2 measurement. The structures they obtained were 23 and 41 nm. Their results showed the potential of ZnO for gas measurement.

1.2.7.2.4 Green synthesis

Green synthesis is the production of nanostructures from plants, living organisms or plant-derived materials. With this method, non-toxic nanostructures are obtained. In this way, it is a promising method for nanostructure synthesis without using expensive and harmful chemicals. [63].

Chen et al. [71] obtained ZnO nanoparticles using *Scutellaria baicalensis* root extract as a reducing agent. As a result of the synthesis, they obtained 50 nm sized particles and concluded that this root extract is capable. Then they tested its photocatalytic performance on methylene blue. According to the test result, they achieved approximately 98% removal in 210 minutes.

1.2.7.2.5 Co-precipitation

Co-precipitation method is a method used to obtain high purity nanostructures. In this method, metal salts are mixed with an alkaline material to obtain precipitate. It is then washed and dried. Can be calcined according to the condition [68,63].

Adam et al. [72] obtained ZnO nanoparticles using low temperature precipitation method. According to their study, they succeeded in producing pure nanoparticles and tested their photocatalytic properties according to pH change. They used congo red as pollutant material. As a result of the photocatalytic test, they achieved 85% removal in 120 minutes.

1.2.7.2.6 Microwave assisted combustion

Microwave assisted combustion method is preferred for high selectivity and chemical yield. With this method, metal oxide nanostructures can be produced rapidly, saving energy and time. In this method, high-frequency electric fields, microwave electric fields are used to heat dipolar materials that have difficulty in aligning [68, 48].

Chen et al. [73] obtained different shapes (sheet, rod, tube) structures using microwave-assisted hydrothermal method and used these structures to photodegrade methyl orange. They compared their results with commercial ZnO particles. As a result, the ZnO structures synthesised by microwave assisted method gave better results.

1.2.8 Limitations zinc oxide

ZnO is a very suitable candidate for photocatalyst considering its durability, environmental friendliness, low cost, and chemical and physical properties [61]. However, despite this versatility, it has some disadvantages. One of the main limiting factors is the recombination of electron-hole pairs. Recombination means that electron-hole pairs recombine rapidly, and the energy of electron-hole pairs is lost

Table 1.2: Synthesis method of ZnO and properties.

Method	Precursor	Advantages	Size (nm)	Structure	Referance
Sol-gel	Zinc Acetate D.	Large surface area, low price, simplest, stability.	30	nanoparticle	[65]
	Zinc Acetate D.		82	nanoparticle	[66]
Hydrothermal	Zinc Acetate D.	Low-price, high stability, simplest, high efficieny.	41	nanorod nanoflower	[70]
	Zinc Chlorine		46	nanoparticle	[69]
Thermal decomposition	Zinc Acetate D.	low-price, high efficiency, don't using toxic solvent.	35	nanoparticle	[67]
Green Synthesis	*Scutellaria baicalensis* extract	non-toxic, environmentally, low-price.	50	nanoparticle	[71]
Co-Precipitation	Zinc Acetate D.	high purity, simplest, high efficiency.	18	nanoparticle	[72]
Microwave-assisted	Zinc Acetate D.	high selectivity, high chemical stability, low price, shorten.	66	nanosheet, nanorod, nanowire	[73]

when they recombine rapidly [74]. This causes a decrease in photocatalytic efficiency. Photocatalytic reactions are based on the separation of electron-hole pairs and their participation in the target reaction.

Another limiting factor is the wide band gap energy. Band gap energy can be defined as the energy difference between the valence band and the conduction band. If this energy is wide, higher energy photons are needed. ZnO has the ability to absorb photons in the UV light region and has a low ability to absorb lower energy photons in the visible region. As a result, it causes a decrease in the use of solar energy. In addition, ZnO can create agglomeration problems at the nanoscale. In this case, it may reduce the photocatalytic efficiency by reducing the surface area exposed to light [75-76].

One of the limiting factors is that ZnO undergoes photocorrosion when exposed to UV light for a long time. Photocorrosion causes dissolution of the photocatalyst during the reaction and the photocatalytic efficiency and stability decrease [76]. The main cause of dissolution was shown to be the reaction between oxygen and positively charged

holes on the ZnO surface. In his study, Gerischer explained the photocorrosion reaction equations with equations 1.11-1.14 as follows [77].

$$O^{-2}_{surface} + h^{+}_{VB} \rightarrow O^{-}_{surface} \quad (1.11)$$

$$O^{-}_{surface} + 3O^{-2}_{surface} + 3h^{+}_{VB} \rightarrow 2\left(O\text{-}O^{-2}\right) \quad (1.12)$$

$$2Zn^{+2} \rightarrow 2Zn^{+2}(aq) \quad (1.13)$$

$$ZnO + 2h^{+}_{VB} \rightarrow Zn^{+2} + {}^{1}/_{2}\, O_2 \quad (1.14)$$

1.2.9 Strategies of improvement the photocatalytic efficiency of ZnO

As can be understood from the information given, the efficiency of a photocatalyst is directly proportional to the electron-hole pair production. For this reason, many modifications have been made to increase the electron-hole pair production of ZnO and to prevent recombination [61]. In order to improve the photocatalytic properties of ZnO, many methods such as morphology control, metal doping, nonmetal doping, semi-metal doping, composite structure formation have been widely tried [76].

ZnO exists in one two, three dimensional nanostructures. Depending on the selected synthesis method and ambient factors, the structures formed vary. The known fact is that 1-D structures have the highest surface area [78]. The increase in surface area is directly proportional to the increase in photocatalytic efficiency. Abinash Das et al. [78] have shown that nanorod structures increase the surface defects and increase the surface area. Thanks to these properties, nanorod structures are one of the structures showing the highest photocatalytic efficiency. It has also been shown that photocatalytic activity increases with increasing aspect ratio. Xinyu Zhang et al. [79] proved this with their study. They compared nanorods with different aspect ratios and the photocatalytic efficiency increased as the aspect ratio increased.

1.2.9.1 Metal doping

As mentioned above, metal doping is very frequently used to eliminate the limiting factors experienced by ZnO. Fe, Mg, Cu, Mn, Ni elements are frequently used for metal doping [61]. Metal doping increases the ion concentration and creates electron traps. It plays a role in reducing recombination [80]. Adam et al. [81] succeeded in doping Mg into ZnO nanoparticles. As a result of their photocatalytic test, a significant

increase in photocatalytic performance was achieved. According to the mechanism they propose, it helps to reduce recombination by exchanging Zn^{+2} and Mg^{+2} in the crystal structure. Increasing the amount of additive too much caused ZnO particles to cluster and resulted in a decrease in photocatalytic efficiency [82]. Kezhen Qi et al. [83] successfully doped transition metals Mn, Fe, Cu, Co, Ni into ZnO structures in order to examine the effect of doping transition metals on photocatalytic efficiency. As a result of their study, Cu-ZnO showed the highest photocatalytic effect. All of the other additives had a higher yield than pure ZnO. They showed that this situation is due to the fact that Zn^{+2} and Cu^{+2} or transition elements create new energy levels and reduce recombination as a result of acting as electron holders.

1.2.9.2 Non-metal doping

Another doping method is doping with non-metal elements. It has been shown that adding non-metallic substances such as carbon, nitrogen, sulfur, fluorine, and boron increases the photocatalytic efficiency in visible light. These materials affect the band gap of ZnO and help increase photocatalytic activity by creating defects on the surface and reducing the possibility of forming recombination centers [61, 84].

Tang et al. [85] successfully synthesized N-doped ZnO and tested its photocatalytic activity on methylene blue. According to the experimental results, they reported that N doping reduced the band energy. The reason for this is that N's 2p electrons create defects near the valence band of ZnO. This situation facilitates the flow of valence band electrons to ZnO. In this way, it helps increase photocatalytic activity. According to the photocatalytic results, N-doped ZnO structures showed a higher photocatalytic efficiency compared to pure ZnO structures.

Ramalingam et al. [86] synthesized sulfur and fluorine doped ZnO nanostructures and tested their photocatalytic properties on methylene blue. According to the study, the effect of sulfur additive on band gap energy is greater than that of flora. There was a decrease in the band gap between the two additives, resulting in the elimination of methylene blue under visible light.

1.2.9.3 Semi – conductor doping

The semiconductor coupling method is widely used to suppress the recombination phenomenon. Thanks to different energy levels and band gap energies, semiconductors

can achieve high photocatalytic efficiency by forming heterojunctions. Mardikar et al. [87] obtained a composite nanoflower structure using the CuO-ZnO hydrothermal method. Then, they performed a photocatalytic test on methylene blue using visible light. They reported a removal of approximately 98% within 30 minutes. They reported that the increase in photocatalytic efficiency is a result of the increased surface area and p-n type heterojunction formation with the flower structure.

Mugunthan et al. [88] synthesized ZnO-WO_3 photocatalyst using the hydrothermal method and used it for the removal of the pharmaceutical compound diclofenac under light. As a result of the study, WO_3 band gap energy decreased and absorption moved to the visible region. In addition, since WO_3 is resistant to acid, it increased photostability. The same result was obtained with 4 repeated cycles.

1.2.9.4 ZnO photocatalyst immobilization

Stable adhesion of photocatalysts to the surface is of great importance for photocatalytic efficiency. Thanks to its fixed presence on the surface, it can interact with pollutants, reduces photocorrosion and supports the photocatalyst by increasing stability [61]. For the most suitable support, it should have a high specific surface area, be sticky, provide strong adsorption and not block the photocatalyst [89]. The most common materials that support ZnO can generally be classified as glass, silica, clay and polymers. Borosilicate glasses are one of the most widely used support materials because they are temperature resistant [90]. In addition, it exhibits the highest peak by XRD for the hexagonal nanorod structure on the glass surface, which indicates that the nanorods are upright and absorb UV radiation and reduce recombination thanks to their polar surfaces [91]. Silica is widely used as a support because it is porous, economical, non-toxic, has a large surface area, stability, high adsorption and increases the efficiency of separating photogenerated charge carriers [92]. Polymeric materials have attractive properties such as being inert, stable, low cost and easily available, and for this reason they have begun to be intensively researched [93-94]. As the final material, clay has high adsorption properties, high stability, chemical resistance, reusability and low cost [95]. It has become interesting because it has high adsorption and may lead to increased surface contact. For these reasons, it can be used as an effective support [96].

1.2.10 Boron doping effect

Boron is a group III element like Al, Ga and In. The doping of these elements into the ZnO structure shows low resistivity and n-type conductivity [97]. Among Group III elements, boron has the lowest ionic radius (0.23 Å), the highest electronegativity (2.04 pauling) and the highest acid strength (10.7) [98]. Due to these properties, it enables the physical and chemical development of the ZnO structure. Having a low radius increases the surface area and acid strength can help improve stability. Additionally, boron can be a powerful radiation shielder [99 - 100].

Kayani et al [101], boron-doped ZnO films were deposited using the dip-coating method and information was collected on the effect of boron percentage on dip-coated boron-doped nanostructured zinc oxide thin films using boric acid as boron precursor. According to the experimental results, it was found that the crystallite size decreased with increasing B contribution. It is observed that the band gap decreases with increasing doping, but at approximately 9%, the band gap increases due to weight B-B clustering. These B-doped ZnO thin films with high transparency and wide bandgap have been noted to be the best for solar cell window and solid-state illumination. As a result of this study, Boron-doped ZnO structures can be used in applications such as electro-capacitors, solar cells and photocatalysis.

Atay et al. [100] successfully produced boron-doped ZnO nanofilms by sol-gel and spin coating and examined their morphological, structural and photocatalytic properties. They performed the photocatalytic test on the pollutant methylene blue. According to the results, element B caused disruption in the crystallization level of pure ZnO films and inhibited crystal growth along the c-axis, while small grains showed that boron-doped ZnO nanofilms exhibited better photocatalytic properties by increasing the active surface area. The reasons for this can be shown as increasing surface area and decreasing band gap energy.

Furka et al [97], successfully added boron to ZnO nanoparticles and wanted to learn the photodegradation of organic dyes using UV-A light. As a result of their experiments, they saw that the band gap energy improved and they attributed this to the ionic diameter of boron reducing the size of the resulting structure. Boron-doped ZnO nanoparticles showed a higher photocatalytic activity than pure ZnO nanoparticles.

Wang et al. [102], prepared sheet spherical boron doped ZnO by hydrothermal technique on a PET-ITO flexible substrate at low temperature (90 °C) and tested its photocatalytic properties. The photocatalytic degradation experiment was performed with a solution of reactive yellow 15 (RY 15, an iron-free azo dye). The photocatalytic properties of ZnO nanostructures were improved by boron doping, thus increasing the degradation rate from 20.4% to 41.45%. This was due to the following two reasons: an increasing number of electron carriers were involved in the redox reactions, and increasing the built-in electric field further separated the photoinduced electron-hole pair, so that the contents of the holes, O^{-2} and •OH as strong oxidants, expanded, leading to increased photocatalytic efficiency.

Sharma et al. [103] synthesized boron-doped and undoped ZnO using the hydrothermal method. Their aim is to develop photoelectrodes to separate water with solar energy. As a result of their study, they showed that the band gap was adjusted according to the doping percentage of the samples and proved the existence of oxygen defects with photoluminescence results. Boron-doped ZnO has been shown to have a better photocurrent with a result of approximately 318%. Increasing surface defects and increasing photocurrent can increase photocatalytic efficiency.

As can be understood from these studies, doping boron can have positive photocatalytic effects on ZnO. It has the potential to be used as a photocatalyst thanks to its effects such as increased surface area, surface defects, and size reduction.

1.2.11 Hypotesis

Water treatment with photocatalysis method, which is one of the advenced oxidation processes, is desired due to its low cost and elimination of pollution. Photocatalysis takes place in the presence of light and photocatalyst. ZnO is a metal oxide semimetal used as photocatalyst. ZnO has restrictive properties such as wide band gap, fast recombination, response to high energy photons. By improving these properties, it is necessary to increase photocatalytic efficiency by using visible region light in terms of energy saving. It is predicted that boron doping can eliminate these limiting factors and improve electrical properties. By using Taguchi method, optimum conditions can be determined with minimum number of experiments and cost in certain factors and level ranges.

2. MATERIALS AND METHOD

2.1 Materials

Zinc acetate dihydrate ($Zn(CH_3COO)_2 \cdot 2H_2O$), Zinc nitrate hexahydrate ($Zn(NO_3)2 \cdot 6H_2O$), Hexamethylenetetramine ($C_6H_{12}N_4$), boric acid (HBO_3), Ethanol %99, methylene blue ($C_{16}H_{18}CIN_3S \cdot xH_2O$) used in this study were obtained from Sigma Aldrich.

2.2 Synthesis of ZnO Nanorods

In this study, zinc oxide nanorods were grown on glass using the hydrothermal method. This method realized two steps. These are seeding on glass with spin coating method and growth ZnO nanorods. For the growth of ZnO nanorods, a seed layer was created on the glasses using the spin coating method. Pure ZnO nanorods were produced using the method developed by Öztürk et al. [104].

2.2.1 Seeding on glass

At this stage, firstly, our microscope glasses (Isolab microscope slides) were cut into 1cm x 2cm dimensions. Then, the cut glasses were cleaned with acetone, ethanol and ultrapure water, respectively, by keeping them in an ultrasonic bath for 10 minutes each. In order to obtain a smooth structure and create a homogeneous surface, seed layer coating was applied on the glass using the spin coating method. The spin coating method helps the surface become more homogeneous thanks to the centrifugal force created by the rotation speed. 0.001 M Zinc acetate dihydrate ($Zn(CH_3COO)_2 \cdot 2H_2O$) was added to 50 ml 99% pure ethanol. Then, it was mixed on a magnetic stirrer for approximately 40 minutes at 60 °C. Afterwards, one of the clean glasses was placed in the spin coating device. 0.3 ml of the prepared solution was dropped onto the glass surface and rotated at 2500 rpm for 20 seconds. Then, the taken glass was dried at 130 °C for 5 minutes. This process was repeated 5 times and finally the resulting glasses

were annealed at 300 °C for 1 hour. In this way, our seed layers were prepared. These thin film layers will create a dipole force on the surface for growth to occur. In this way, ZnO nanorod growth will occur with the attraction created by this electric field.

2.2.2 Growth zinc oxide nanorods

ZnO nanorod growth was carried out under pressure and temperature using the hydrothermal method. The hydrothermal method thus enabled the growth of crystal structures from the liquid phase. For the hydrothermal growth solution, equal molar (0.01 M), Zinc nitrate hexahydrate ($Zn(NO_3)2{\cdot}6H_2O$) and Hexamethylenetetramine ($C_6H_{12}N_4$) were mixed in 80 ml of ultrapure water at room temperature for 1 hour. Hexamethylenetetramine is a water-soluble, nonionic amine group. Its main role here is to provide hydroxyl ions that interact with Zn^{+2} to form ZnO [105-106]. After the mixing process was completed, the solution was transferred to a bottle and our glasses with the seed layer were added to the bottle with the help of an apparatus. The glass bottle was tightly closed and kept at 90 °C for 3 hours. Meanwhile, growth took place on the seed layer-covered glass surfaces under the influence of temperature and pressure. Then, the glasses where the growth took place were taken, washed with pure water and allowed to dry.

2.3 Synthesis boron doped ZnO

In this study, boron addition was carried out during the growth phase. The material used for boron additive is boric acid (HBO_3). For the hydrothermal growth solution, equal molar (0.01 M), Zinc nitrate hexahydrate ($Zn(NO_3)2{\cdot}6H_2O$) and Hexamethylenetetramine ($C_6H_{12}N_4$) are mixed in 80 ml of ultrapure water at room temperature for 1 hour, while boric acid is left to stir in ultrapure water. Dissolved boric acid is added to the hydrothermal solution at 1,3,5,7,10% wt (B-ZNO-1, B-ZnO-3, B-ZnO-5, B-ZnO-7, B-ZnO-10). Then, the processes applied to growth ZnO nanorods were applied in the same way. As a result of these processes, six different samples will emerge. The synthesis stages are shown in Figure 2.1.

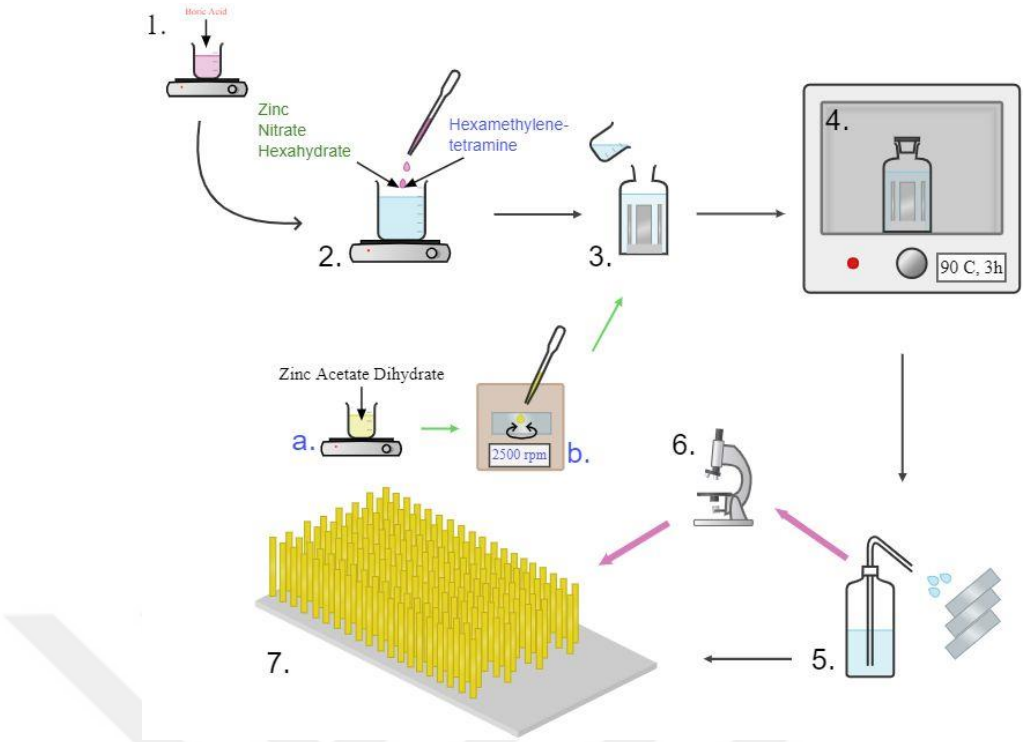

Figure 2.1: Synthesis of B-ZnO Nanorods 1. Prepare boric acid solution, 2. Prepare hydrothermal solution with adding boric acid, 3. Pour the prepared solution into the flask with the glasses, 4. Bottle keep in oven at 3 hour 90 °C, 5. Cleaning glass, 6. Using microscope, 7. Boron doped ZnO nanorods, a. prepared seed layer solution, b. cover the glass with spin coating.

2.4 Characterization of ZnO Nanorods and B-ZnO Nanorods

In this study, X-Ray diffraction (XRD) and Fourier Transformed Infrared Spectroscopy (FT-IR) devices were used for structural analysis. XRD (Rigaku, smartlab) analysis was used to determine the crystal structures of the obtained samples. In this method, X-ray is sent to the sample. The X-ray is reflected from the sample surface to obtain a diffraction pattern. By examining this diffraction pattern, the phase of the sample, crystal lattice parameters (c) and grain size can be calculated. The samples were made with CuKa1 (λ =0.15406) radiation in the range 2θ=25-80 and at room temperature. Particle size calculation was calculated using the Debye-Scherrer equation given in Equation 2.1. For grain size, the angle in the plane and the full maximum half width (FWHM) values of the plane were used.

$$D = \frac{K\lambda}{\beta_{hkl} \cos\theta} \tag{2.1}$$

In Equation 15, D refers to the particle size or crystal size. K is the Scherrer constant and its value is approximately 0.9. λ is the wavelength of the incident X-ray (0.15406 nm). β represents FWHM in radians. θ is the Bragg scattering angle. Bragg's law in Equation 2.2 is used to calculate crystal parameters.

$$n\lambda=2d_{hkl}\sin\theta \tag{2.2}$$

Here n is the diffraction order and generally n = 1. λ is the wavelength of the incident X-ray (0.15406 nm). d_{hkl} is the space between the planes of the given miller indices h, k, The lattice constant a and c can be related by Equation 2.3:

$$\frac{1}{d_{hkl}^2}=\frac{4}{3}\left(\frac{h^2+hk+k^2}{a^2}\right)+\frac{l^2}{c^2} \tag{2.3}$$

FT-IR analysis is used for structural properties of our samples. This analysis is used to understand the chemical bonds, functional groups and molecular structure within the substance by measuring the absorption properties of a substance in the infrared region. Devices called interferometers are used. This device allows infrared light directed at the sample to be passed through an interferometer, creating a spectral component. In this process, light is separated into different wavelengths and the frequencies absorbed by the sample are measured. In this study, the analysis was carried out with the Jasco FT/IR-4700 spectrometer device at room temperature, in the range of 500-4000 cm^{-1}. UV-Vis spectrometry analysis was used to check its optical properties and absorption capabilities. Optical properties are determined by re-measurement of the light coming from the light source after it passes through the sample or is reflected. While UV-Vis spectroscopy can take measurements in solution, it can also get results from thin films and thin coatings. Thermo Scientific brand Multiskan Go model spectrophotometer was used for this measurement. Measurements were made between 200-800 nm. Band gap energy was calculated with the results obtained from the UV-Vis spectrometer. Optical band gap determination was achieved using the Tauc plot method. Tauc Plot calculation is shown in Equation 2.4.

$$\alpha h\upsilon=A\left(h\upsilon-E_g\right)^n \tag{2.4}$$

Here α is the absorption coefficient, hυ represents the photon energy, Eg is the band gap, A is the proportionality constant, and n represents the transition mode. ZnO has a direct transition mode, therefore it has the value n = ½. Scanning electron microscope

(SEM) analysis was used to examine the surface and topography properties. Scanning Electron Microscope is a type of microscope used to examine and visualise material surfaces at very high magnification. Electron beam is used to obtain high resolution images. Here, a focused electron beam is created to scan the surface of the sample. When the electron beam hits the surface of the sample, signals such as backscattered electrons and characteristic X-rays are emitted from the sample. These signals are collected and processed by the detector. ZEISS Evo LS 10 brand SEM device was used in this study. The analysis was carried out zooming up to 200 n m by keeping the accelerating voltage of 10 kV constant. To examine the electrical properties, DC electrical characterization (I-V) and AC electrical characterization analysis were performed depending on temperature. In I-V analysis, voltage is applied to the sample at 0.05 V intervals, starting from 0 Voltage (V) within a certain time interval. The voltage is increased to 2 V, then reduced to -2 V and increased again to 0 V. This cycle is repeated 2 times. Current values were monitored by applying voltage. Made for temperatures of 19, 27, 40, 60, 80, 100, 120, 140, 160, 180 °C, respectively. Keysight B2901BL Source Measurement Unit was used for DC electrical characterization. Then, AC electrical characterization analysis was carried out for the same temperatures. Hioki IM3523 LCR Meter device was used in this measurement. The device measured at different ranges from 40 Hz frequency to 200 kHz frequency. For AC electrical characterization, an AC signal of a certain frequency and amplitude is sent to the sample being analyzed and how it behaves under this signal is examined. The G (Concuctance) parameter was used in these tests for AC conductivity. The G parameter shows us the conductivity level under AC conditions. Lakeshore 335 Temperature Controller device was used for temperature control.

2.5 Photocatalytic Tests

Photocatalytic tests were performed in a closed environment under UV-A (CAMAG, 8W) light at 366 nm. Methylene Blue was used as the contaminant. Methylene Blue was prepared in 3 different concentrations. The prepared concentrations were $2x10^{-6}$, $1x10^{-5}$ M, $5x10^{-5}$ M, respectively. pH adjustment was made using dilute HCl and NaOH. Each concentration was prepared in the pH range of 4, 7 and 10. The pH range was checked with a pH meter. Then, the prepared Methylene Blue concentrations were transferred to pre-cleaned quartz glasses as 3ml. First of all, to measure the effect of

light on Methylene Blue degradation, Methylene Blue concentrations in the quartz were kept in a light environment for 90 minutes. Using a UV-Vis spectrometer, the concentration change was monitored by establishing the relationship between absorbance change and concentration in equation 2.5. There was no significant degradation in Methylene Blue concentrations when kept under light for 90 minutes. In photocatalytic experiments, 1x2 cm glasses with B-doped and undoped ZnO coated on the surface were added into the quartz. It was kept in a dark environment for 40 minutes for adsorption-deadsorption equilibrium to occur. Then, the samples were left under light for a total of 90 minutes to wait for photodegradation.

$$C_0 = A_0 \tag{2.5}$$

Here C_0 indicates the initial concentration amount, A_0 is the absorbance value corresponding to the initial concentration value. Equation 2.6 was applied for percentage calculation.

$$degredation\ rate\ \% = 1 - \frac{C_t}{C_0} x\ 100 \tag{2.6}$$

Here, C_0 indicates the initial concentration amount, and C_t indicates the concentration amount at time t. Reaction kinetics is compatible with the pseudo first order kinetic model and is shown with the time-dependent graph of $\ln(C_t/C_0)$. The slope of the graph gives us the rate constant (k). Equation 2.7 was used for general kinetics calculation.

$$ln\left(\frac{C_t}{C_0}\right) = -kt \tag{2.7}$$

Here, C_0 indicates the initial concentration amount, C_t indicates the concentration amount at time t, and k indicates the rate constant (min^{-1}).

2.6 Taguchi Method

The Taguchi method was developed by Genichi Taguchi in the 1940s and emerged to increase quality and reduce costs [107]. Taguchi method is an easy and successful technique used to optimize experimental parameters. The Taguchi method uses a special orthogonal array design to investigate all process parameters with a small number of experiments. It offers advantages over classical experimental design methods. The Taguchi method reduces the variation of the outcome variable and shows the best way to find optimum process conditions. It is the best and most economical

way to determine optimum process conditions and increase efficiency in experimental design.

In the Taguhi method, first the problem is selected, then the factors that will answer the problem are determined and their levels are assigned. The factors can be generally examined under two headings. These are controllable and uncontrollable factors. Uncontrollable factors are either very difficult and expensive to control, or impossible to control. However, Taguchi developed a design in which the variance can be minimized by finding appropriate optimal values for controllable factors against uncontrollable factors. Finally, there is the selection of orthogonal arrays. Orthogonal arrays were developed as a mathematical tool. It is used in cases where there are many parameters and levels affecting the system. The purpose of creating orthogonal arrays is to ensure that all factors are included in the modeling with equal trial numbers. The most important reason for the widespread use of orthogonal arrays is that many factors are tested at a minimum scale. In this way, the number of experiments is minimized. Then comes the analysis part of the collected data. Experimental results obtained in the Taguchi method are evaluated by converting them into signal/noise (S/N) ratio.

Signal/noise ratio is a performance statistic that shows the effect of controllable factors and uncontrollable factors on the performance statistic by using the mean and standard deviation together. S/N ratio is calculated and analyzed in different ways according to the targeted value: nominal is best (Equation 2.8), larger is better (Equation 2.9), smaller is better (Equation 2.10).

Nominal is best:

$$\frac{S}{N} = 10 \log\left(\frac{y}{s_y^2}\right) \tag{2.8}$$

Larger is better;

$$\frac{S}{N} = 10 \log\left(\frac{1}{n}\sum_{i=1}^{n}\frac{1}{y_i^3}\right) \tag{2.9}$$

Smaller is better:

$$\frac{S}{N} = 10 \log\left(\frac{1}{n}\sum_{i=1}^{n} y_i^2\right) \tag{2.10}$$

In the equations stated above for S/N ratios, y refers to the performance characteristic value, s^2 refers to the variance, and n refers to the number of experiments.

In this study, four factors were selected and mix level design was used. The selected factors are shown in Table 2.1.

Table 2.1: Factors and levels of Taguchi Design.

Factors/Levels	pH	Concentration (10^{-5} M)	Time (min)	Doped (%wt)
1. Level	4	0,2	30	0
2. Level	10	1	60	3
3. Level		5	90	7

The selection of factors was made according to appropriate design and photocatalytic activity results. In line with the selected levels and factors, the L18 orthogonal array was chosen. So there are 18 experiments. The selected factors are pH, time, concentration and additive amount, respectively. The answer sought for these factors is the amount of degradation. It is based on the fact that bigger is better. The Table 2.2 shows us the experiments.

Table 2.2: Experimental precedure of Taguchi Design.

pH	Time (min)	Concentration (10^{-5} M)	Doped (%wt)
4	30	0,2	0
4	30	1	3
4	30	5	7
4	60	0,2	0
4	60	1	3
4	60	5	7
4	90	0,2	3
4	90	1	7
4	90	5	0
10	30	0,2	7
10	30	1	0
10	30	5	3
10	60	0,2	3
10	60	1	7
10	60	5	0
10	90	0,2	7
10	90	1	0
10	90	5	3

3. RESULT AND DISCUSSION

3.1 Structural Properties of Materials

In order to examine the structural properties of ZnO, B-ZnO-1, B-ZnO-3, B-ZnO-5, B-ZnO-7, B-ZnO-10 nanorods synthesized within the scope of this study, XRD measurements at an angle of 25-80˚degrees and FTIR analyzes were carried out. The resulting diffraction patterns are given in Figure 3.1. Using the diffraction patterns and the values taken from them, 2θ, FWMH, lattice parameter, crystal size of the (002) peak are given in Table 3.1.

When the obtained patterns and peak positions were examined, it was concluded that the samples had a hexagonal wurtzite structure (JPCDS No. 36-1451). While the (002) peak was dominant in all samples, the (100) peak began to be observed with the increase in the amount of dope. The (100) peak started to become evident with 3% contribution. It ended with a 7% contribution. This indicates that the crystal lattice expands in the a direction. This peak, which appears around 2θ=32˚, matches the hexagonal wurtzite structure and shows growth in the a direction. This peak was not observed at 10% contribution. No impurity peaks arising from doping or any other element appeared in the synthesized samples. B^{+3} (0.23 Å) has a lower atomic diameter than Zn^{+2} (0.74 Å). A shift to lower angles is expected with the replacement of B atoms and Zn atoms. A shift in the angles may indicate successful doping [108]. Additionally, according to Wang et al., they reported that there may be shifts in the peaks due to B ions settling in octahedral cavities [102]. Shifts in the peaks also serve as evidence that defects have occurred. The crystallite size calculated according to the Scherrer formula is given in the Table 3.1. What is expected due to boron doping is that the crystal size decreases as the doping amount increases. It was observed that the crystal size decreased partially with 1%, 5% and 10% additives. An increase is observed in samples with 3% and 7% additives. There are no big differences in the crystal sizes of the other samples. Lattice parameters also showed values close to each other.

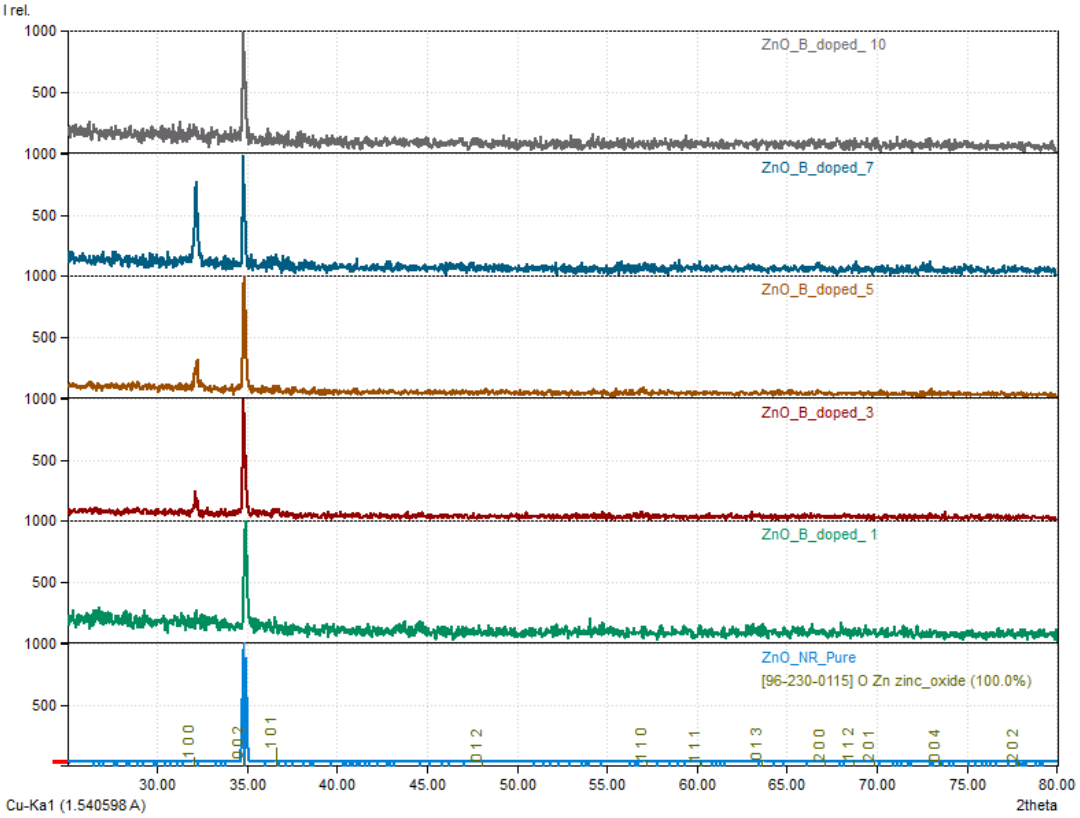

Figure 3.1: XRD results of ZnO, B-ZnO NRs.

Table 3.1: 2θ, FWHM, lattice parameter (c), crystal size (D) values of samples.

Sample	$2\theta_{(0\,0\,2)}$	$FWHM_{(0\,0\,2)}$	C (Å)	D (nm)
Pure ZnO NR	34,868	0,18143	5,139239	45,898
B-ZnO NR-1	34,861	0,19628	5,136403	42,428
B-ZnO NR-3	34,854	0,17254	5,141551	48,261
B-ZnO NR-5	34,86506	0,18479	5,138206	45,064
B-ZnO NR-7	34,844	0,15263	5,142961	54,555
B-ZnO NR-10	34,843	0,1907	5,141179	43,665

FT-IR spectra can be used to confirm that the B dopant is included in the ZnO structure. In this study, the results of pure ZnO, 3% and 5% doped samples were examined. FT-IR spectroscopy of B-doped and undoped ZnO nanorods were measured in the range of 500-4000 cm^{-1} and can be seen in figure 3.2 FT-IR results. According to the FT-IR results, some important peaks emerged. The resulting peaks between 500-1039 cm^{-1} are attributed to the Zn-O structure. The peaks between 1300-1700 cm^{-1} are attributed

to B-O, B-O-B structures. As can be seen from Figure 3.2, as the amount of additive increases, the precision of the peaks increases. From here we can conclude that the doping was successful. In addition, if the O-H band peaks appearing around 3000 cm^{-1}, we can interpret that the sample is hydroxylated. In this way, it may have contributed to the increase of photocatalytic efficiency because hydroxyl groups may have acted as adsorption centers [99,109].

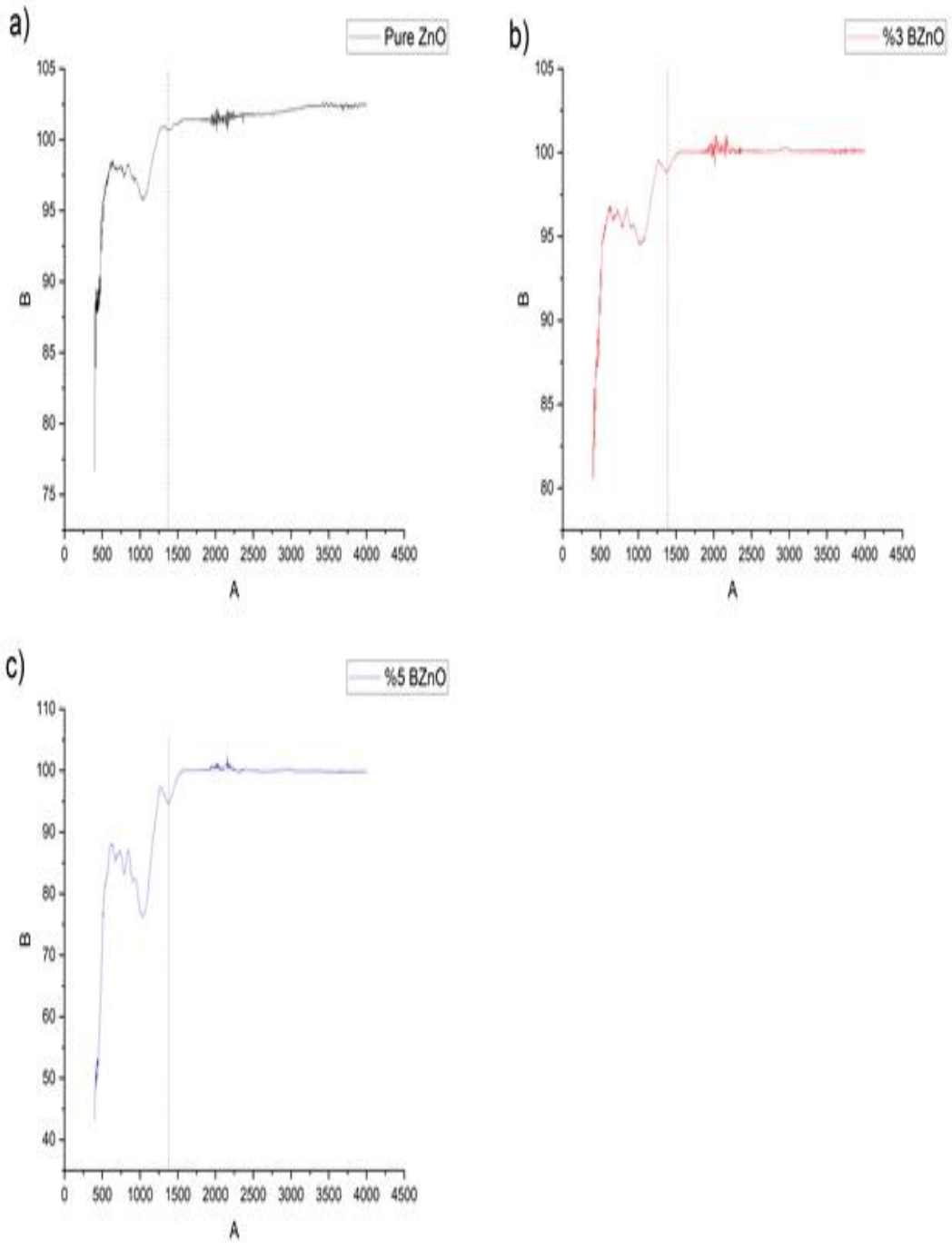

Figure 3.2: FT-IR results of a) pure ZnO, b) %3 B-ZnO, c) %5 B-ZnO Nanorods.

3.2 Optical Absorption of Materials

The optical properties of the synthesized B-doped and pure samples were measured with UV-Vis. UV-Vis absorption spectra of pure and B-doped ZnO measured in the 200-800 nm wave range are shown in the Figure 3.3. According to the results obtained, ZnO, B-ZNO-1, B-ZnO-3, B-ZnO-5, B-ZnO-7, B-ZnO-10 samples, 352 nm, 361 nm, 362 nm, 359 nm, It gives a sharp absorption peak around 363 nm and 364 nm. As can be seen from the values, a red shift, that is, an absorption peak towards the visible region, was observed with the boron contribution among the samples.

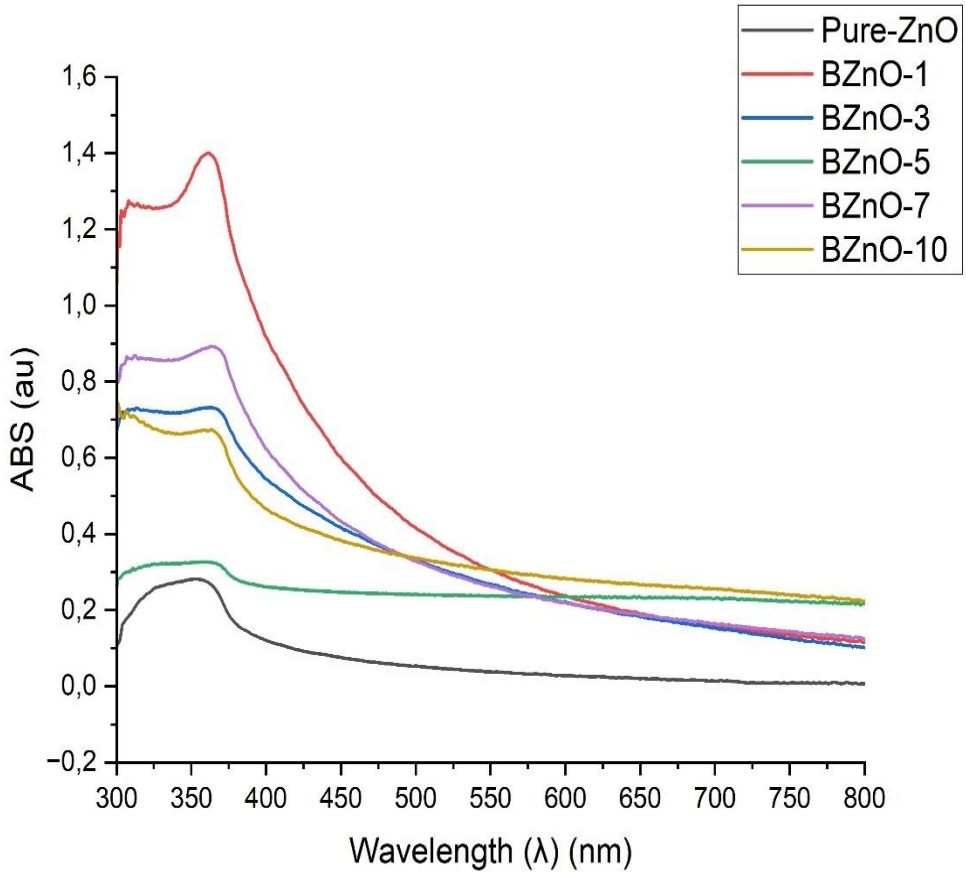

Figure 3.3: UV-Vis specktrometer results of all samples.

Band gap energy was calculated from the peaks obtained by applying the Tauc method. The shift in absorption peaks was also successfully reflected in the band gap energies. The band gap energies for ZnO, B-ZNO-1, B-ZnO-3, B-ZnO-5, B-ZnO-7, B-ZnO-10 samples respectively were calculated as 3.22 eV, 3.10 eV, 2.97 eV, 3.06 eV, 3.06 eV, 3.11 eV. Graphs showing band gap energies are given in the Figure 3.4.

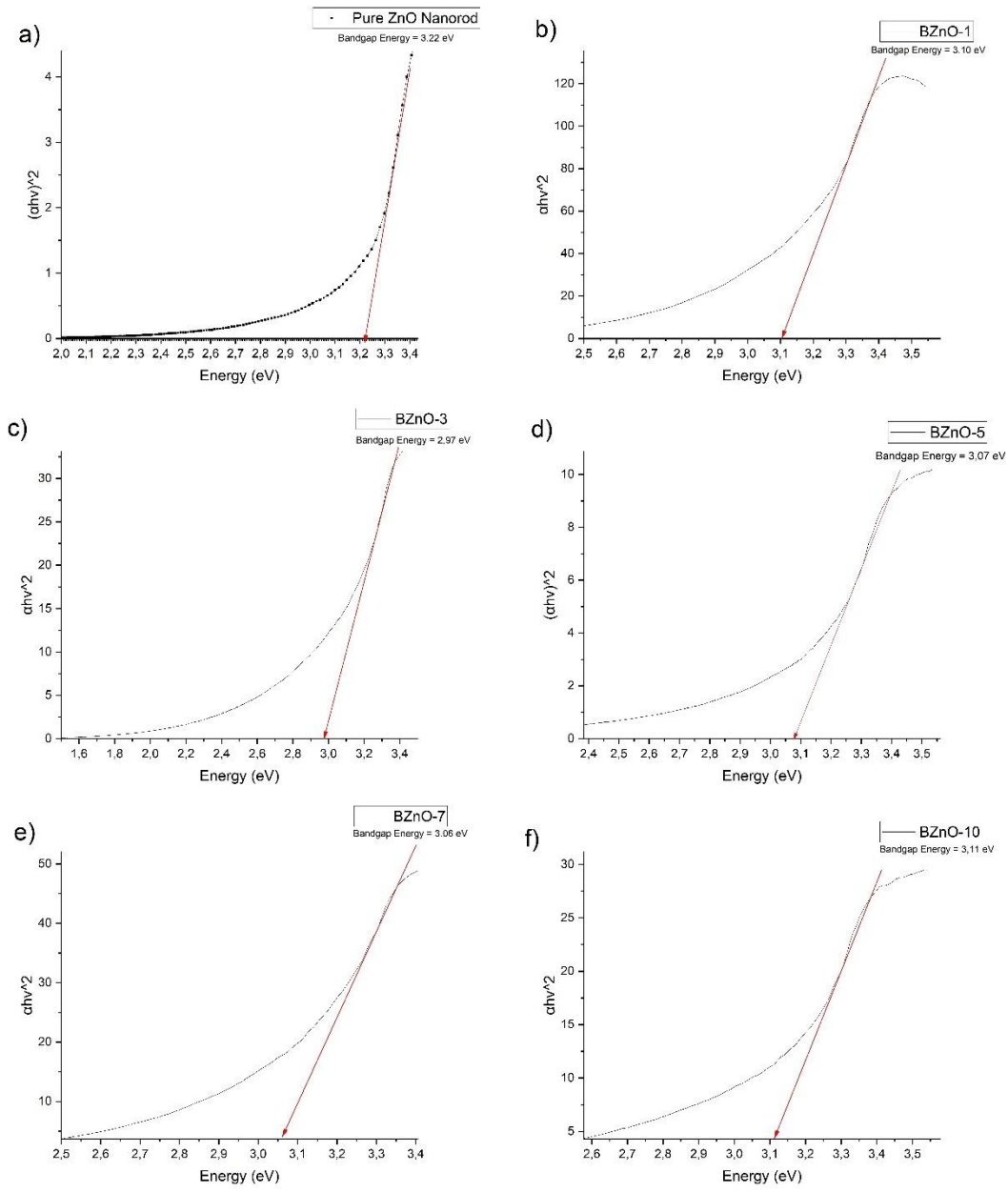

Figure 3.4: Band gap energies calculated as a result of the Tauc method a) pure ZnO, b) %1 B-ZnO, c) %3 B-ZnO, d) %5 B-ZnO, e) %7 B-ZnO, f) %10 B-ZnO.

Salas et al. [99] showed that the adsorption peaks of boron doping shifted towards the visible region, and the band gap energy decreased by revealing new energy levels as electrons occupied the conduction band in doped ZnO. Furka et al. [97], with the doping, adjacent bands are formed and the energy decreases for the transitions between the valence band and the conduction band. We see the result of this in the band gap energy and absorption peaks. According to these results, the best band gap energy is found in 3% B-doped ZnO. 3% and other boron doped samples have lower band gap energy compared to pure ZnO.

3.3 Morphological Properties of Materials

In order to check the surface properties of the obtained samples, images were taken using a scannin electron microscope. These images are shown between Figure 3.5, 3.6, 3.7, 3.8, 3.9, 3.10. As can be seen from the images, nanorod growth was successful. Hexagonal wurtzite structure formation was observed for all samples. Although there are gaps on the surface, coating and nanorod growth were achieved. When we examine in more detail, the average diameter of pure ZnO nanorods is around 55 nm while their length is around 900 nm. It is observed that nanorod diameters decrease with increasing doping amount. Especially towards 10% doping amount, the average diameter decreases to around 35 nm and the average length decreases to around 450 nm. This situation revealed by SEM images proves that the surface area increases with the decrease in nanorod diameters. SEM results also show that the XRD particle sizes we obtained are in good agreement. We also know that Zn^{+2} and B^{+3} are replaced by Zn^{+2} in the ZnO lattice structure as the doping amount increases. This situation changes the electric field, which is necessary for nanorod growth, resulting from dipole forces. In this case, it creates a restrictive effect on nanorod growth. According to the XRD results, we can say that the (100) peak increasing with the doping amount is due to this electric field. Our SEM results support our XRD results and show the effect of boron doping.

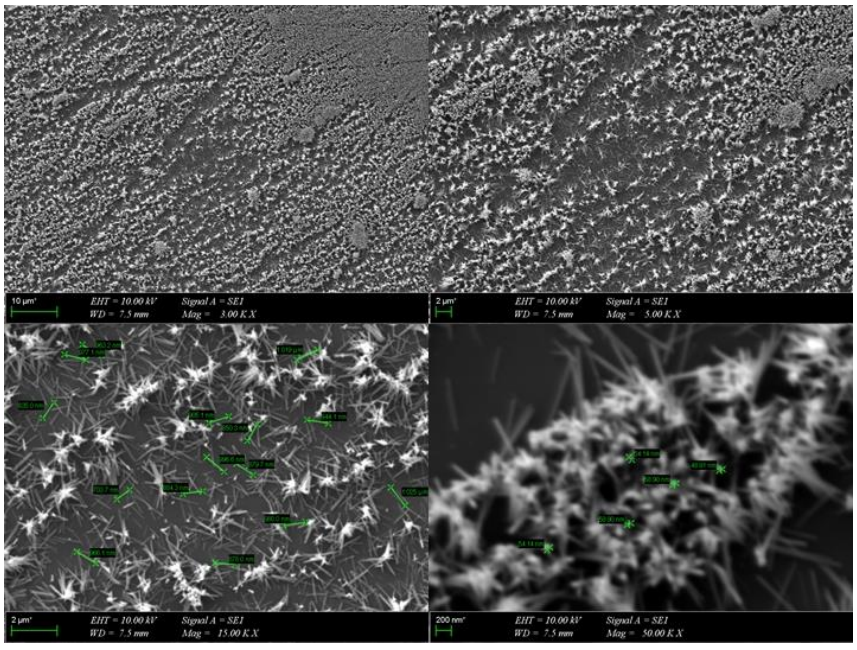

Figure 3.5: SEM images for pure ZnO nanorods.

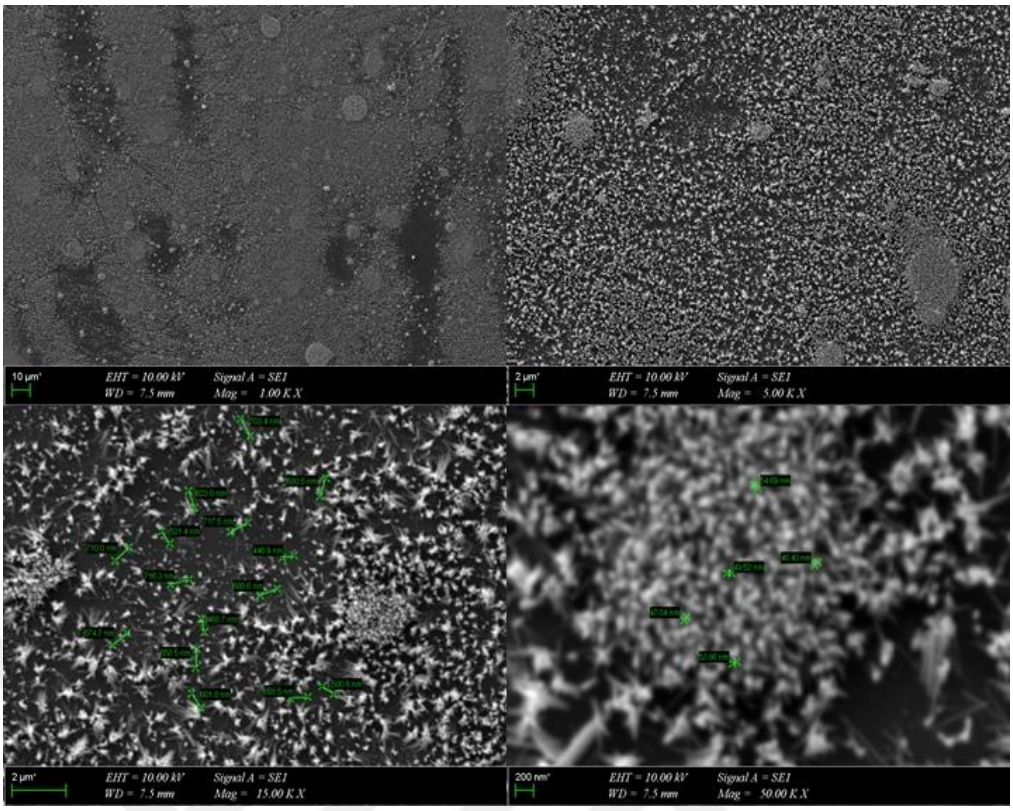

Figure 3.6: % 1 B-ZnO structures for SEM images.

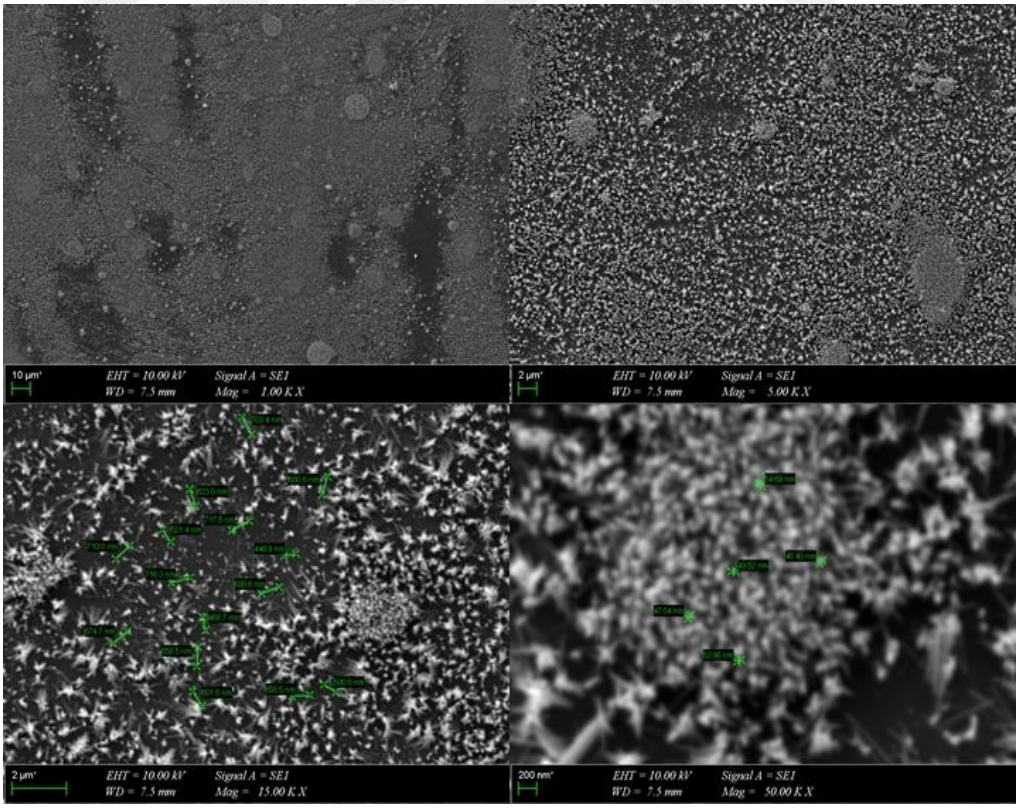

Figure 3.7: %3 B-ZnO structures for SEM images.

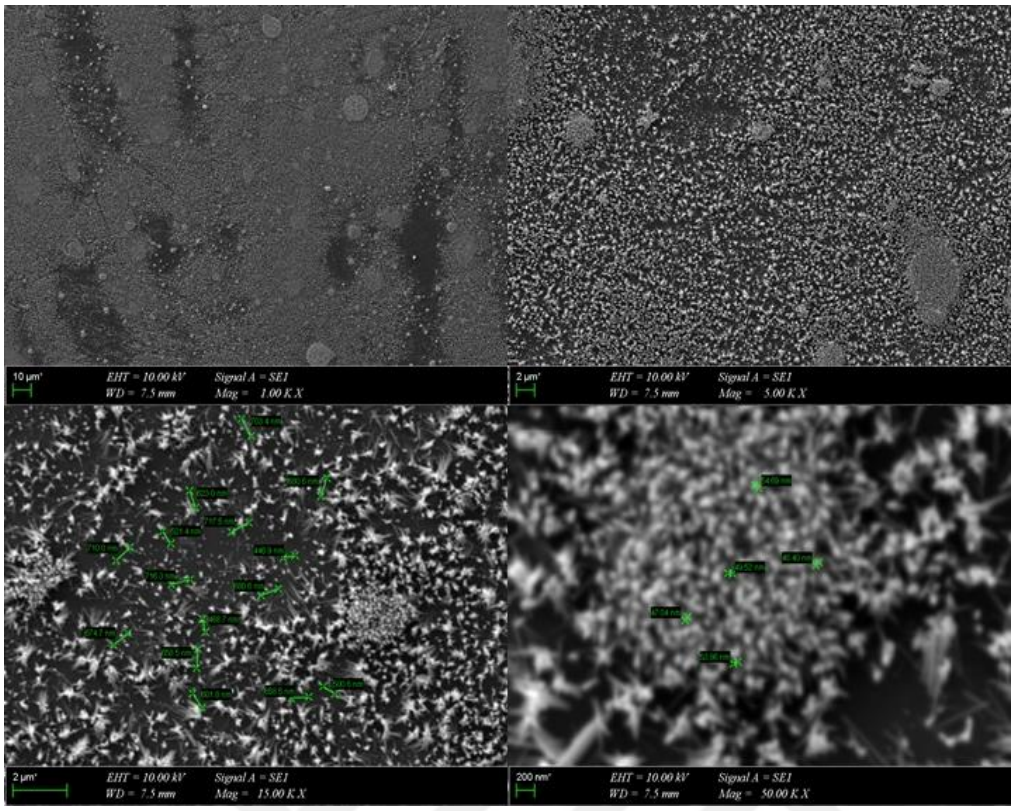

Figure 3.8: %5 B-ZnO structures for SEM images.

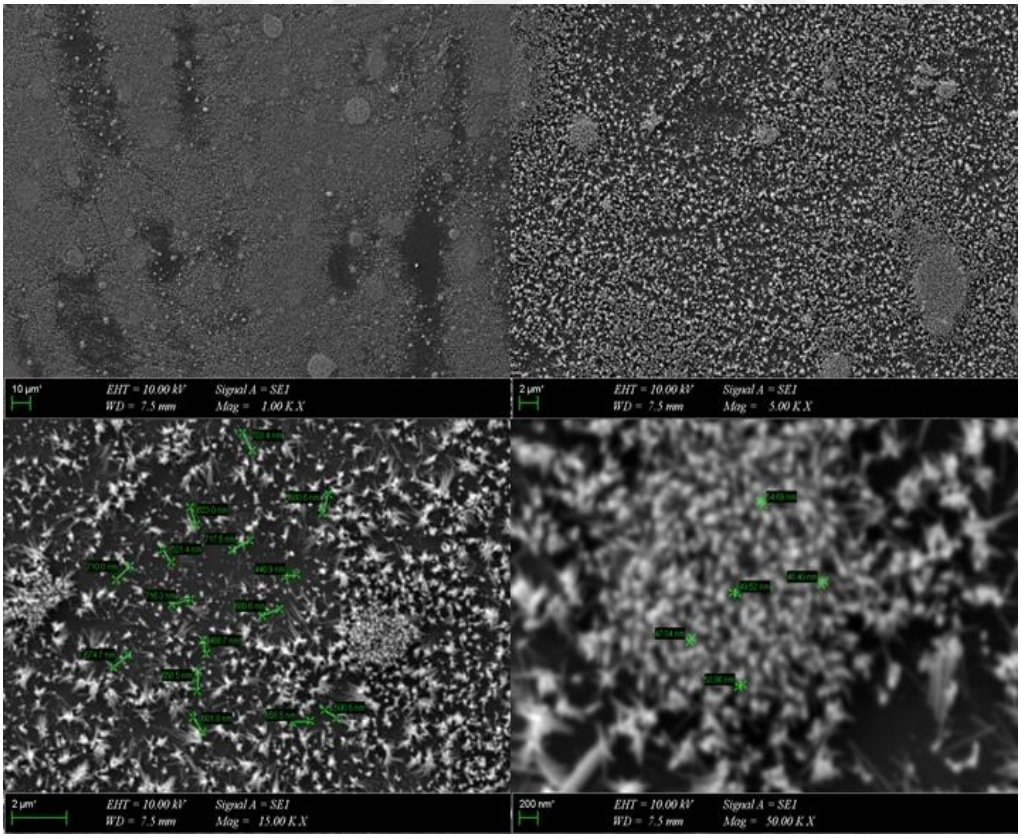

Figure 3.9: %7 B-ZnO structures for SEM images.

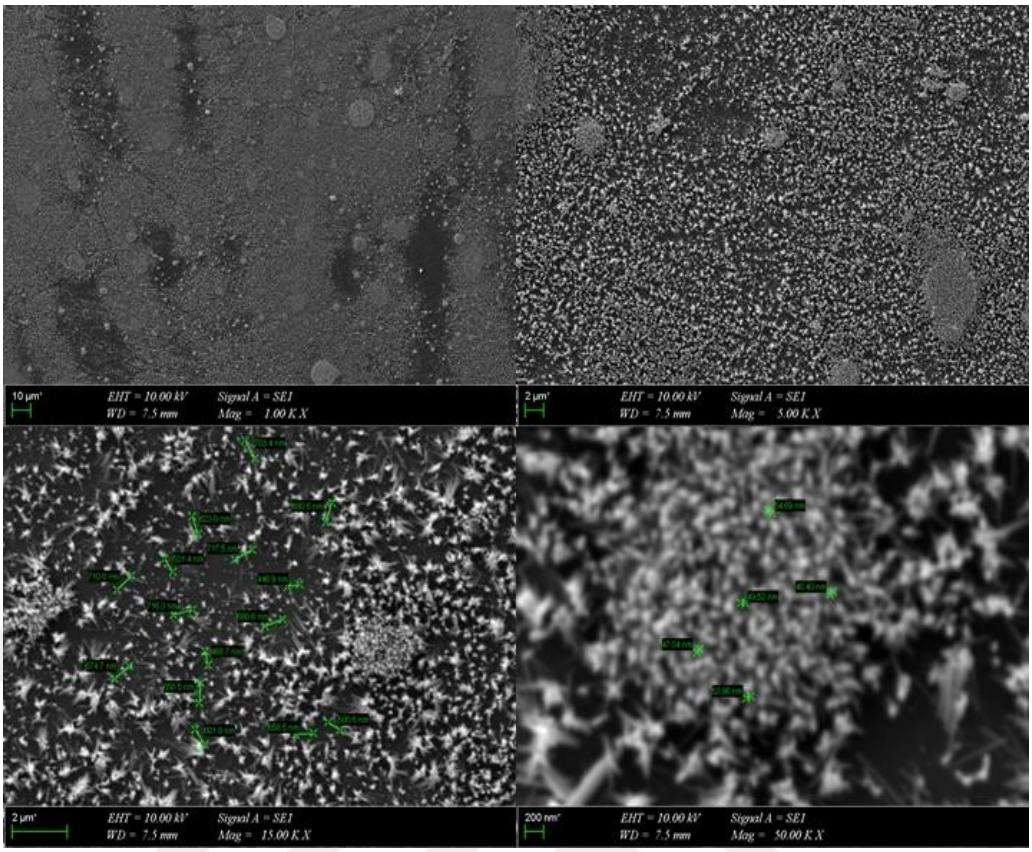

Figure 3.10: %10 B-ZnO structures for SEM images.

3.4 Electrical Properties

The electrical properties of the obtained samples, pure ZnO nanorod, 3% B-doped nanorod and 10% B-doped nanorods, and the temperature-dependent changes of DC and AC currents were examined and discussed. Measured in nitrogen environment. During the measurements, 200 standard cubic centimeters per minute (sccm) of high purity N_2 gas was flowed through the measurement cell.

In DC characterization, we apply voltage up to 2 V to the samples in steps of 0.05 V, starting from 0 at certain time intervals. When the voltage reaches 2V, we reduce it symmetrically to -2V, then come back to 0 V. We repeat this cycle twice and monitor the voltage and current changes one by one for each temperature. Figure 3.11 (a-c) represents the Current-Voltage (I-V) characteristic graph for these samples at 19, 80, 140, 180˚C. Figure 3.11 shows the graphs of Figure 3.11a pure ZnO, Figure 3.11b 3% B-doped ZnO, and Figure 3.11c 10% B-doped ZnO. It is valid for all three graphs that the current value gradually increases as the voltage increases. When we examine the

graphs of boron-doped samples, we see that the current increases with the amount of doping. With 10% contribution, the current value increased approximately 5 times.

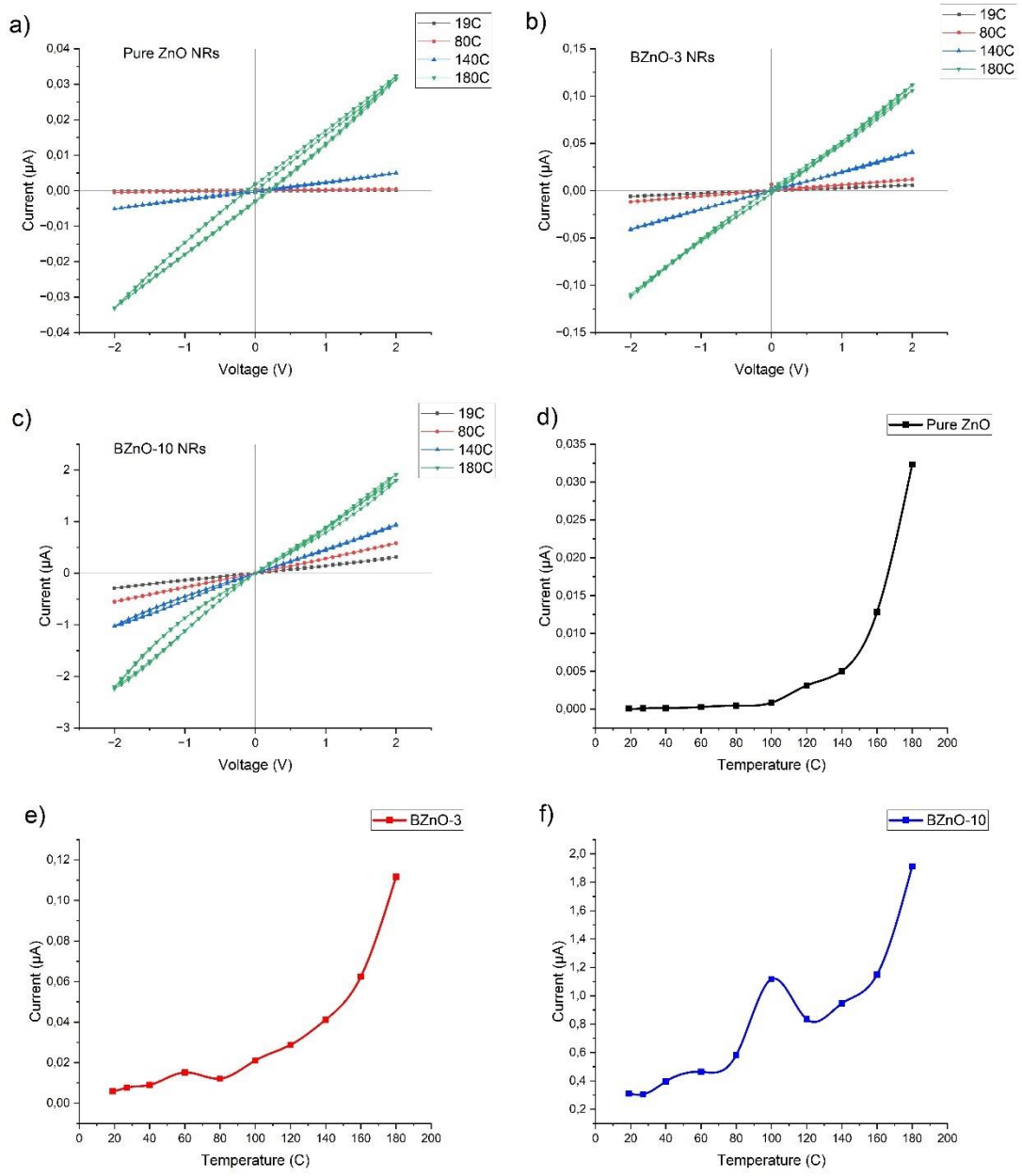

Figure 3.11: a) I-V results of pure ZnO, b) I-V results of 3%B-ZnO, c) I-V results of 10% B-ZnO, d) temperature-dependent current of DC for pure ZnO, e) temperature-dependent current of DC for 3% B-ZnO, f) temperature-dependent current of DC for 10% B-ZnO.

ZnO is an n-type semiconductor material [110]. When we examine the graph in Figure 3.11d, the current for pure ZnO shows a sharp increase with the increase in temperature. This is a typical semiconductor behavior [111]. Figure 3.11e and 3.11f are the current-temperature graphs of samples with 3% and 10% B added, respectively.

Pure ZNO in Figure 3.11d shows an exponential behavior. As the amount of doped increases, this behavior turns from exponential to linear form. We can make the following comment from this situation. During the formation of ZnO, the boron mineral restores the electrons that were taken from the crystal structure by oxygens to the ZnO crystal structure and changes the type of conductivity behavior from semiconductor form to metallic form depending on the contribution rate. However, it should not be forgotten that with increasing temperature, the electrical conductivity of metals decreases instead of increasing. Our interpretation here is that boron doping changes the electrical conductivity behavior of ZnO by giving electrons to its crystal structure. Figure 3.12 shows the change in AC conductivity of pure ZnO, 3% and 10% B-doped samples, respectively, according to temperature.

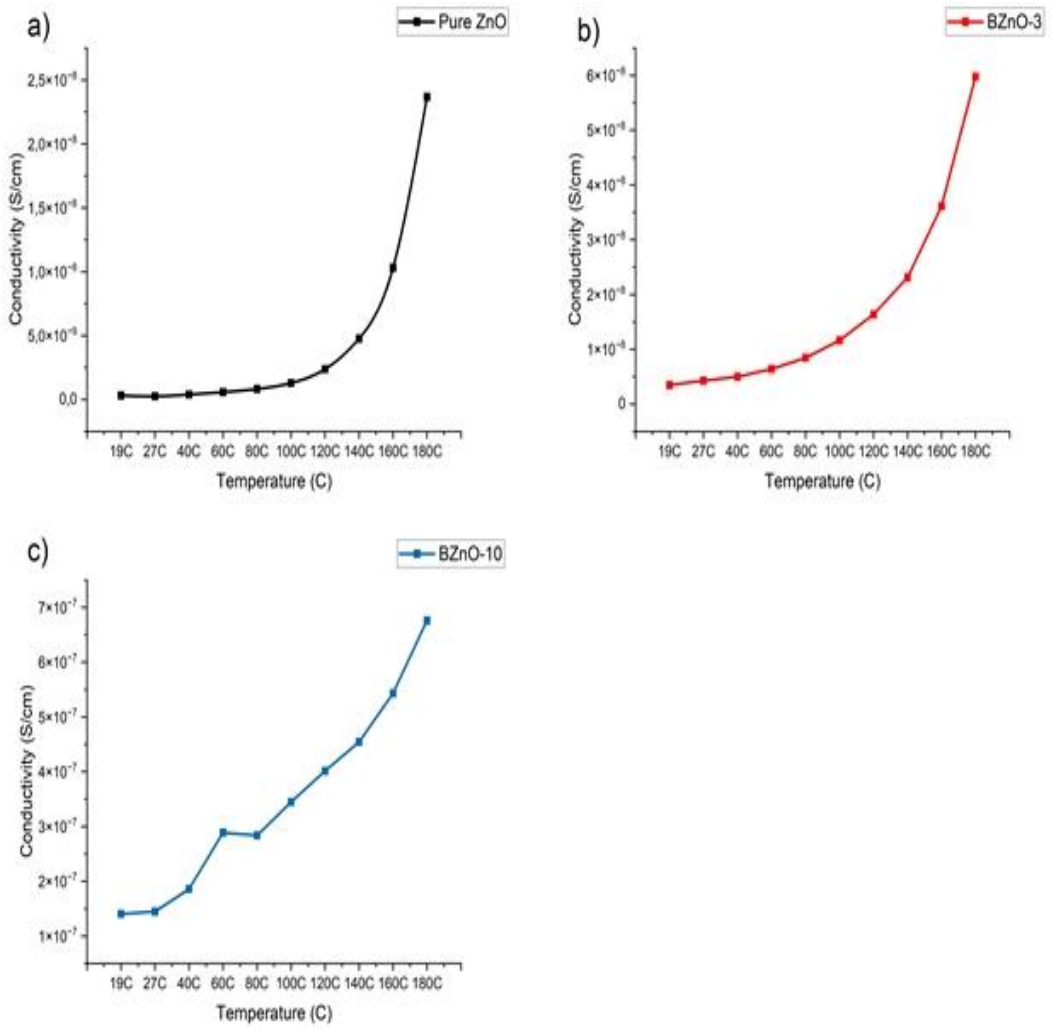

Figure 3.12: a) Temperature dependent current of AC for pure ZnO, b) temperature dependent current of AC for 3% B-ZnO, c) temperature dependent current of AC for 10% B-ZnO.

While calculating these changes, the G parameter was used for AC conductivity. The G parameter tells us the conductivity level. As in the graphs given in DC electrical characterization, in AC electrical characterization graphs, a transformation into linear form occurs with the increase in B contribution. This situation shows us that there is a transition from the semiconductor conductivity form to the metallic form. As we mentioned before, ZnO is an n-type semiconductor material. Exponential increase for pure ZnO is also an expected response in this case. As seen in Figure 3.13, it is seen that the conductivity increases as the boron contribution increases for these measurements.

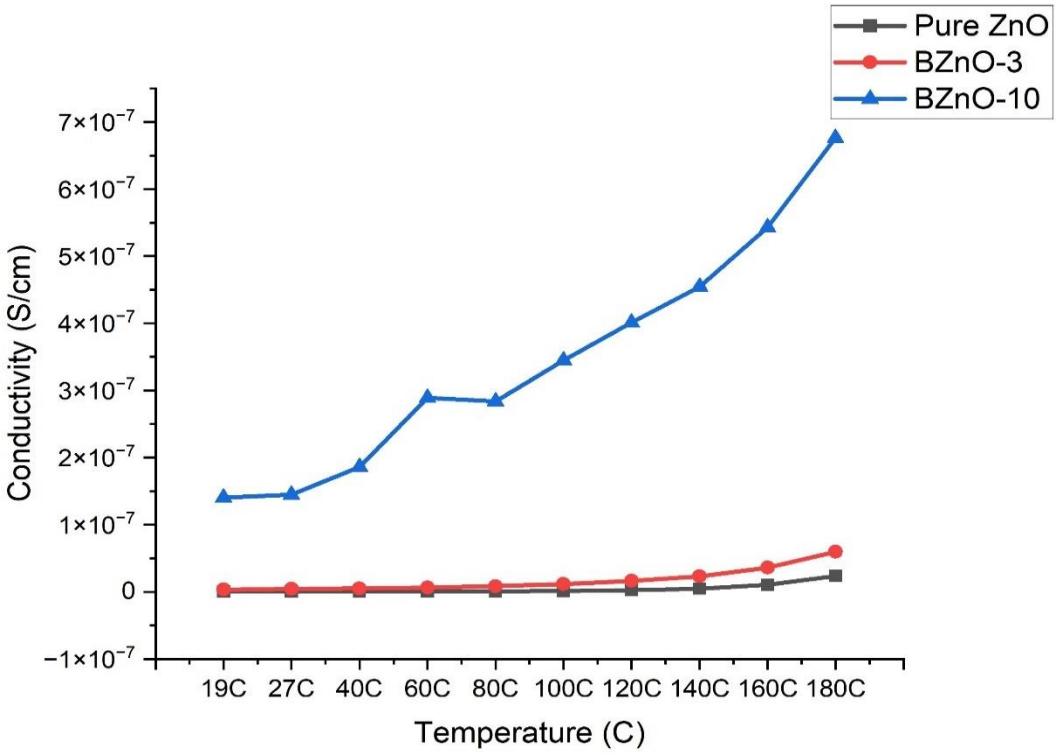

Figure 3.13: Temperature dependent AC current for pure ZnO, %3 B-ZnO, %10 B-ZnO.

Maximum, pure ZnO showed a conductivity value of 2.37×10^{-8} S/cm, 3% B-doped ZnO 5.98×10^{-8} S/cm, 10% B-doped ZnO 6.76×10^{-7} S/cm. Compared to pure ZnO, 10% B-doped ZnO showed an increase of approximately 300%. As can be understood from here, the electrical properties of ZnO change with the addition of boron and the conductivity increases. Increasing conductivity results in an increase in the ability to donate and transport electrons to the medium, and photocatalytic efficiency is expected to increase.

3.5 Photocatalytic Test Results

To examine the photocatalytic properties, B-doped and undoped samples with an area of 2 cm^2 were vertically immersed in MB solutions at different pH (4, 7, 10) and concentrations ($2x10^{-6}$, $1x10^{-5}$, $5x10^{-5}$ M). Negligible degradation occurred as a result of exposing methylene blue to catalyst-free irradiation. pH is an important factor in photocatalysts produced for aqueous solutions. The response of the photocatalyst may vary depending on the pH range. The pH range also has an effect on the response of the pollutant used. Therefore, pH plays an important role both in the properties of dyes and in the reaction mechanisms that can contribute to dye degradation, namely hydroxyl radical attack, direct oxidation by the positive hole, and direct reduction by the electron in the conduction band [112]. Additionally, ZnO can be rapidly eliminated or photocorroded in acidic environments. For this reason, we wanted to see what effect the amount of additive would have on pH.

Photocatalytic tests were first carried out by keeping the samples containing photocatalysts in the dark for 60 minutes and waiting for them to reach adsorption-deadsorption equilibrium. Then, it was left under UV-A irradiation for 90 minutes and photodegradation was expected at the end of the process. Figure 3.14 shows us the time-dependent graphs of $\ln(C/C_0)$ values according to pH levels at the end of 90 minutes. Based on these graphs, slopes and rate constants were found. Rate constants are given in the Table 3.2. As can be seen from the obtained graphs, Methylene blue concentrations decreased as light exposure time increased. Here, we have shown that photodegradation occurred successfully. When we examined the rate constants obtained from the slope of the graphs, 3% B-doped ZnO nanorods showed the best results for $2x10^{-6}$ M concentration with a rate constant of 0.00856 min^{-1}. For $1x10^{-5}$ M concentration, 7% B-doped ZnO nanorods showed the best results with a rate constant value of 0.00665 min^{-1}. Finally, for $5x10^{-5}$ M concentration, the 3% doped sample showed the best result with a rate constant value of 0.00308 min^{-1}. In addition, if we compare the numerical values of the rate constants for 1x10-5 M concentration according to Table 3.2, for pH 4, the 1% B doped sample has a 94% higher rate than the pure ZnO sample. For pH 7, the 3% B-doped sample has a 36% higher rate than pure ZnO, and finally for pH 10, the 7% B-doped sample has a 194% higher rate constant. We can say that rate constants actually show us the effect of efficiency. When the Table 3.2 is examined, almost all doped ZnO nanorods showed higher values than

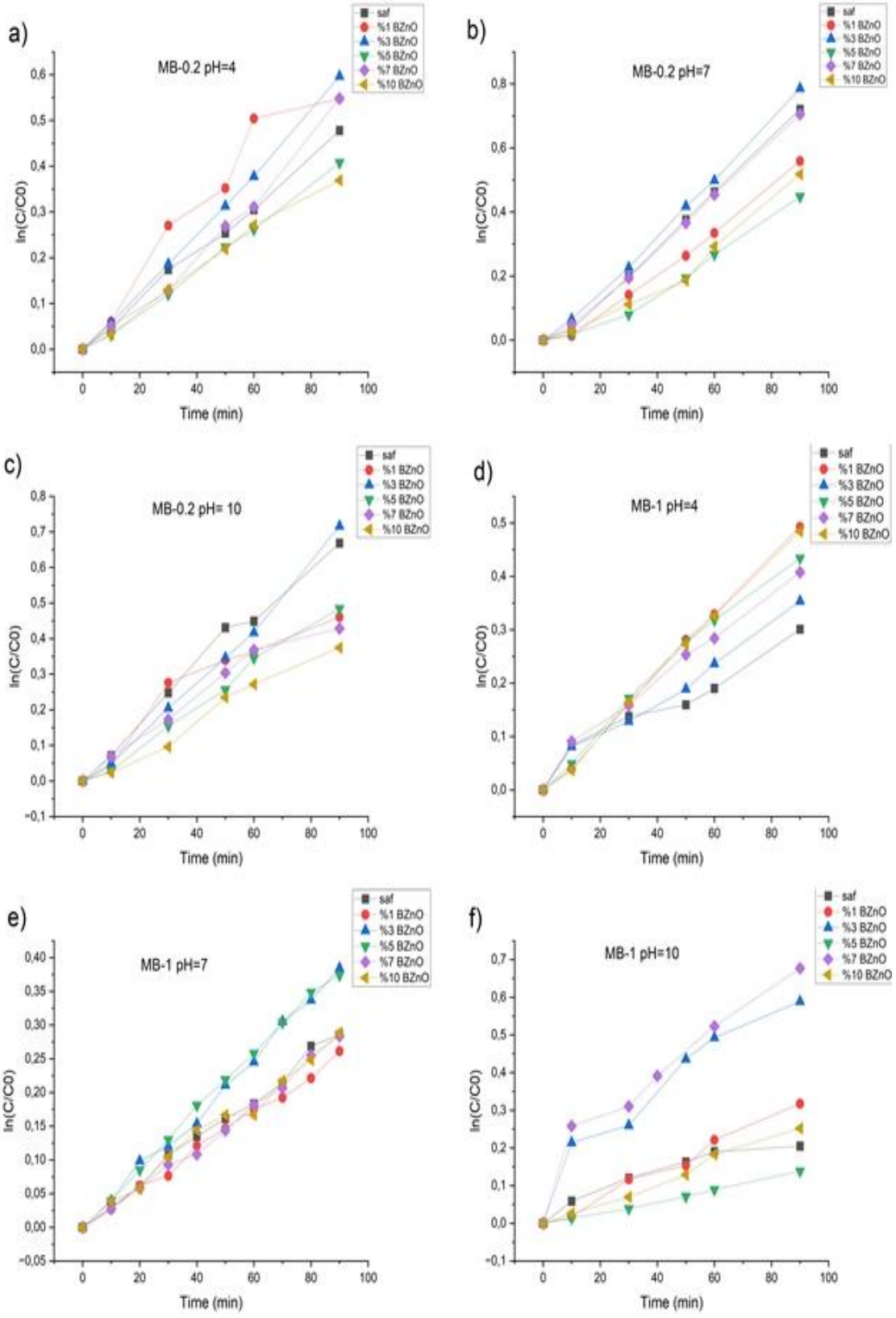

Figure 3.14: Graphs all sample of pseudo first kinetic models, a) time-dependent ln(C_0/C) graphs for 2x10^{-6} M methylene blue, pH4, b) pH7, c) pH10, d) time-dependent ln(C_0/C) graphs for 1x10^{-5} M methylene blue, pH4, e) pH7, f) pH10, g) time-dependent ln(C_0/C) graphs for 5x10^{-5} M methylene blue, pH4, h) pH7, i) pH10.

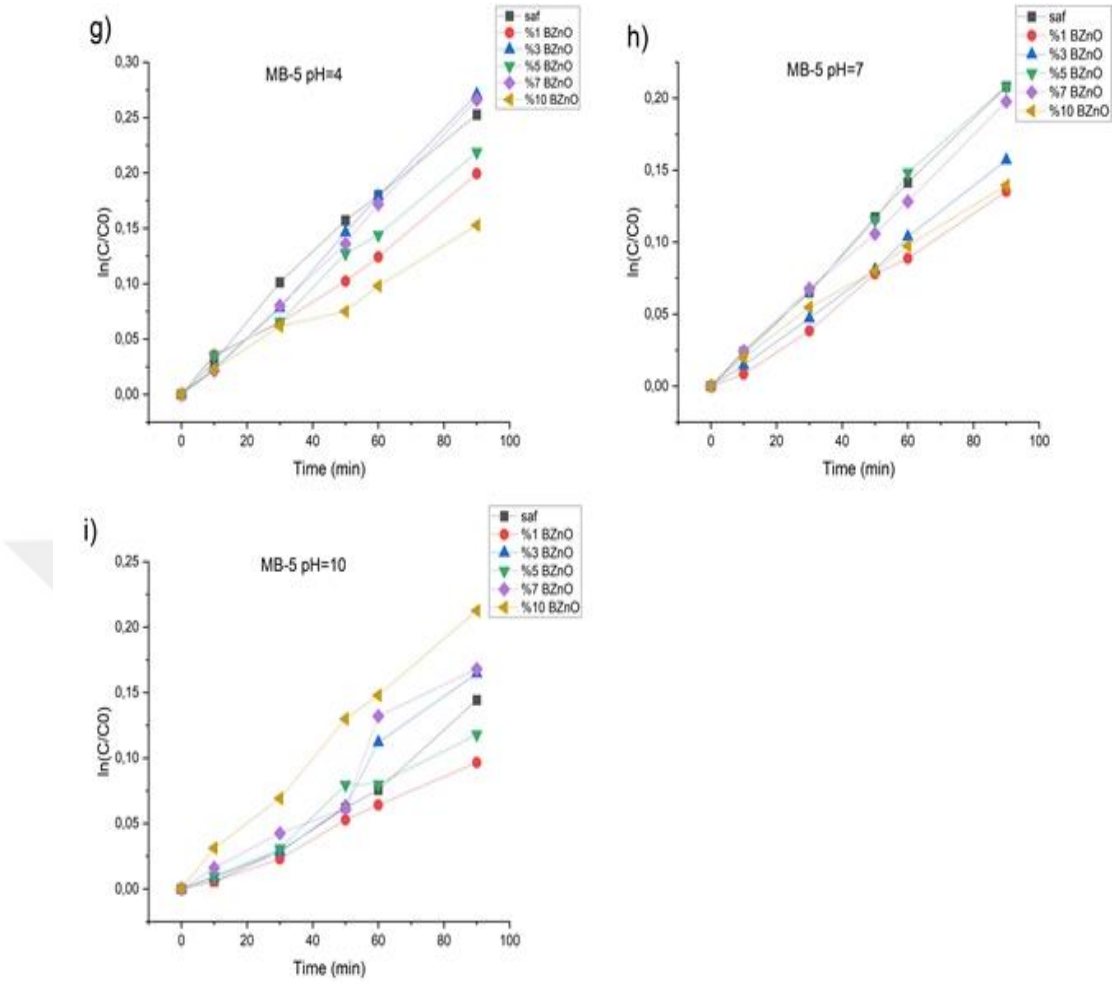

Figure 3.14 (continue): Graphs all sample of pseudo first kinetic models, a) time-dependent ln(C_0/C) graphs for 2x10^{-6} M methylene blue, pH4, b) pH7, c) pH10, d) time-dependent ln(C_0/C) graphs for 1x10^{-5} M methylene blue, pH4, e) pH7, f) pH10, g) time-dependent ln(C_0/C) graphs for 5x10^{-5} M methylene blue, pH4, h) pH7, i) pH10.

ZnO nanorods for every pH range and concentration range. Samples with 5% doping exhibited low photocatalytic performance at different pH and methylene blue concentrations. The reasons for this may be due to reasons such as rapid recombination, inhomogeneous surface, agglomeration, and lack of adhesion to the surface. Moreover, if we ignore the 5% B-doped ZnO nanorods, the Table 3.2 shows that 10% B-doped ZnO nanorods also exhibit poor performance. Only pH value 10, at 5x10-5 concentration and pH value 4, at 2x10-6 M concentration appeared to be higher than other values. It has a low rate constant for all remaining methylene blue concentrations. 3% and 7% amounts of boron doped by mass showed the best results.

Table 3.2: Rate constant of pure and B doped Samples.

pH=4			
Conc	0,2	1	5
Pure	0,00521973	0,0028796	0,0028422
1%	0,00651619	0,0055767	0,00209828
3%	0,00673143	0,0035914	0,00307792
5%	0,00458881	0,004937	0,00239041
7%	0,00615259	0,0042887	0,00301613
10%	0,00424834		0,00161713
pH=7			
Conc	0,2	1	5
Pure	0,00834306	0,0031906	0,00232851
1%	0,00633211	0,0028426	0,00155016
3%	0,00855899	0,0042495	0,00175404
5%	0,00505756	0,0042687	0,0023589
7%	0,00810856	0,0031443	0,00216072
10%	0,00565244	0,0030769	0,00153304
pH=10			
Conc	0,2	1	5
Pure	0,00775898	0,0022638	0,00157119
1%	0,00529552	0,0035988	0,00111339
3%	0,00774992	0,0057358	0,00196516
5%	0,0055851	0,0015374	0,00137502
7%	0,00524017	0,006655	0,00201488
10%	0,00443306	0,0028678	0,00236783

The improvement of photocatalytic activity with boron doping can be associated with the suppression of recombination of electron-hole pairs by increasing surface defects. F. Atay and his colleagues showed that boron doped increases surface defects as a result of photoluminescence test [100]. B dopant serves as electron transporter for reduction-oxidation reactions [113]. In addition, it increased the photocatalytic efficiency thanks to its wide spread on the surface and increasing the surface area.Wei Wang ve arkadaşları [102] found that B doping increased the photocurrent density compared to pure ZnOs, and they attributed the increase in photocatalytic efficiency to the decrease in the probability of recombination as the photocurrent density

increased. Here, photocatalytic degradation can be attributed to the free radical O_2 anion, •OH radical and electron-hole pairs that can be directly formed. These radicals act as a strong decomposing agent and ensure the degradation of methylene blue. It was said that when the optical properties were checked, there was a red shift in the UV-Vis spectrum and this would have a direct effect on the band gap. While discussing the optical properties, it was stated that there was a decrease in the band gaps of 3% and 7% B-doped samples compared to pure ZnO nanorods. The band gap reduction directly increased the photocatalytic efficiency. Then, according to our electrical analysis results, we proved that the electrical conductivity of B-doped samples is significantly better than pure ZnO for both DC and AC. It can easily be said that as the conductivity increases, the gap between the conduction band and the valence band decreases. This decrease shows us that new levels are formed there and the electron conduction function increases. In this way, more electrons were introduced into the system and the photocatalytic efficiency increased. New levels formed between the conduction band and the valence band may have created electron traps, increasing the electron holding capacity and thus reducing the recombination event. As can be seen from all these results, photocatalytic activity was improved thanks to the B doped.

3.6 Taguchi Design Analysis

Taguchi design is a design method used to obtain the best results at low cost. In this study, the effects of factors on degradation efficiency, the effects of factors on each other, the predictions of factors will be discussed and the results will be interpreted. It has been proven by characterization analyzes and photocatalytic tests that boron doping improves the photocatalytic activity on ZnO nanorods. Our aim is to produce the most efficient photocatalysts under the minimum conditions, and the effects of the factors we have introduced will be explained in detail both on degradation and on dope. The degradations (%) of the experiments encountered with Taguchi design are given in the Table 3.3. Experimental results were calculated in Taguchi analysis, with greater being the best. S/N performance analysis of the factors was calculated according to the Taguchi design method. According to the calculated analysis, the importance of the effect factors are time, concentration, doped, pH, respectively.

Table 3.3: Experimental design of Taguchi method and degredation (%).

pH	Time	Conc	Doped	Degradation (%)
4	30	0,2	0	15,9722
4	30	1	3	12,0636
4	30	5	7	7,6988
4	60	0,2	0	28,2897
4	60	1	3	21,0526
4	60	5	7	15,7898
4	90	0,2	3	43,9402
4	90	1	7	33,4721
4	90	5	0	22,3150
10	30	0,2	7	18,2073
10	30	1	0	11,3136
10	30	5	3	4,8128
10	60	0,2	3	32,0930
10	60	1	7	38,5021
10	60	5	0	7,2901
10	90	0,2	7	44,2969
10	90	1	0	21,5269
10	90	5	3	18,1788

The order of importance for pH was determined as 4 with a very low difference, time was selected as the highest time (90), the lowest concentration was shown as the best and the amount of dope was selected as 7%.

The value order and impact share are shown in the Table 3.4. Then, the main effect plot for the S/N ratio is shown in Figure 3.15. Accordingly, the effect of pH value can be explained as the electrostatic interaction between the catalyst surface and the target pollutant. pH affects the surface state of the catalyst and the ionization state of ionizable organic compounds, thereby affecting the interfacial electron transfer and photoredox process. Additionally, depending on pH, hydroxyl radical production plays an important role in reaction mechanisms that can contribute to pollutant degradation, such as direct oxidation by the positive hole and direct reduction by the electron in the conduction band. It is generally shown that acidic pH has a greater contribution to degrading pollutants. In this study, the pH level of 4, which is acidic, shows compliance with the rule. We can say that time is a critical factor for photocatalytic reactions to occur. As time increases, photocatalytic efficiency increases to a certain point, but when it reaches the saturation point, the efficiency remains constant. In this

study, the time was determined as 90 minutes. Another parameter is concentration. By adjusting the concentration amount, we can increase or decrease the amount of adhesion of pollutants to the surfaces and we can also change the penetration of light by concentration. As a result, high concentrations may accumulate on the photocatalyst surface and reduce the amount of degradation. It can prevent the surface from being activated by blocking light from passing through. In this study, in accordance with what we said, the concentration lower than $2x10^{-6}$ M gave the best results. Finally, the effect of the additive amount was examined. It has been discussed in the previous section that as the amount of B contribution increases, surface defects will increase and the recombination process will be reduced, with the increasing amount of electrons, more electron-hole pairs will be formed and more electron transport will occur, and since the B contribution has a small ion diameter, it will homogenize and increase the surface area. We can understand the accuracy of the results we discussed in this design model from the effect of contribution B. The lowest effect was with pure ZnO, while the highest effect was with 7% B-doped ZnO.

Table 3.4: İmpact of factor and rank value.

Level	pH	Time	Conc	Doped
1	25,91	20,56	29,04	24,18
2	24,87	26,43	26,34	24,99
3		29,18	20,79	27,01
Delta	1,05	8,63	8,24	2,83
Rank	4	1	2	3

ANOVA analyzes were used to examine confidence levels on degradation. In this study, the independent variables are pH, concentration, time and dop amount, while the dependent variable is the amount of degradation as a percentage. With this analysis, error rates were also calculated. Table 3.5 ANOVA results are shown. According to the model, the factors with the highest contribution rates are time (42.08%), concentration (34.63%), doped (8.51%) and pH (0.04%). The error rate of the model was calculated as 14.73%. For ANOVA analyses, P-value becomes meaningful when

it is less than 0.05. In this study, dope amount, time and concentration gain meaning since they have a value less than 0.05.

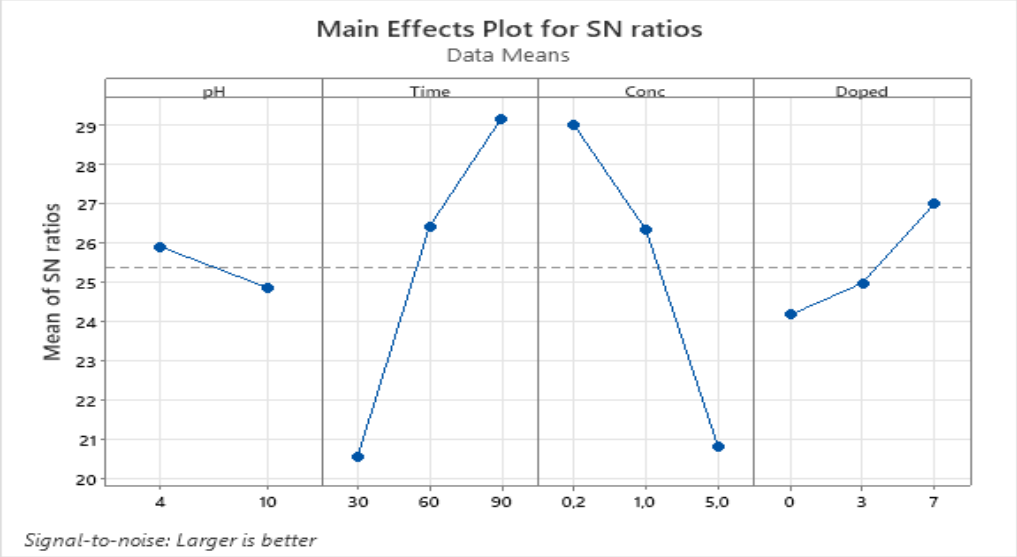

Figure 3.15: The main effect plot for the S/N ratio.

Table 3.5: ANOVA Results.

Source	DF	Seq SS	Adj SS	Adj MS	F-Value	P-Value	Contribution
pH	1	1,06	1,06	1,06	0,04	0,85116	0,04%
Time	1	1076,58	1076,58	1076,58	37,13	0,00004	42,08%
Conc	1	886,01	886,01	886,01	30,56	0,0001	34,63%
Doped	1	217,64	217,64	217,64	7,51	0,01686	8,51%
Error	13	376,89	376,89	28,99			14,73%
Total	17	2558,19					100,00%

The table 3.6 shows the R^2 values. The R^2 value tells you to what extent the data fits the model. The higher the R^2 value, the better the data fits the model. The R^2 value for this study is 85.27%.

Table 3.6: The value of R^2.

S	R-sq	R-sq(adj)	R-sq(pred)
5,38437	85,27%	80,73%	72,83%

The resulting regression equation for methylene blue removal is given in Equation 3.1.

Degredation = 6,53 - 0,081 pH + 0,3157 Time - 3,341 Conc + 1,213 Doped (3.1)

Figure 3.16 normal probability graph is given. Finding our values on or close to the line in the normal probability graph gives us information about the reliability and fit of our model. The normal probability plot for this study shows that the model is compatible.

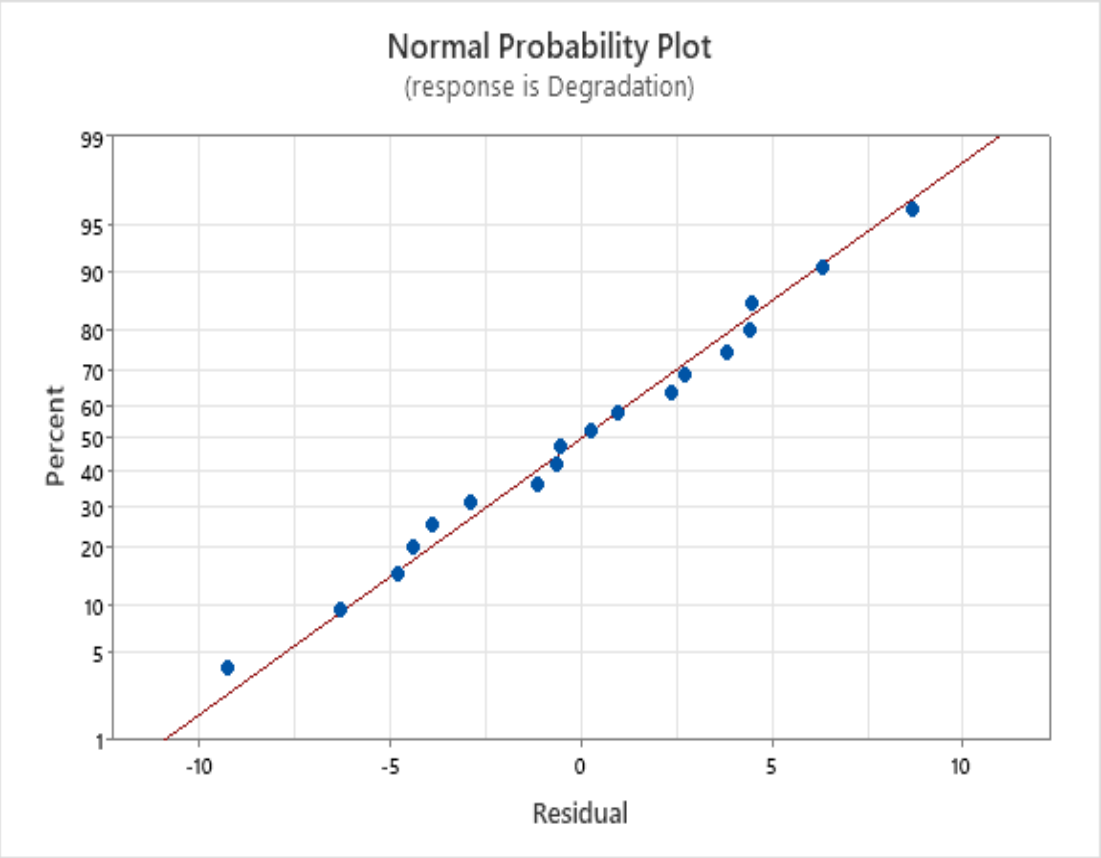

Figure 3.16: Normal Probability Plot.

The Taguchi design, regression equation obtained in this experiment was made using Minitab 16. Estimates of the degradation amounts for the entire experiment by Taguchi Design are also given in the Table 3.7. According to the table 3.7, the best efficiency in our study was achieved with a pH value of 10, a duration of 90 minutes, 7% doped amount at a concentration of $2x10^{-6}$ M, and the highest S/N ratio according to the design was also the highest for this experiment. The estimated degradation values calculated according to the bigger-is-better design in the Taguchi design program were also equivalent to our experimental results, and it is said that the best experimental result was achieved with a pH value of 10, a time of 90 minutes, and a 7% doped amount at a concentration of $2x10^{-6}$ M. The model we implemented with Taguchi design showed us the best result, compatible with its own design parameters.

Table 3.7: The value of predict degredation with Taguchi method.

pH	"Time (min)	Concentration (10-5 M)	Doped (%wt)	Degradation (%)	S/N	Predict Degredation (%)
4	30	0,2	0	15,9722	24,067	16,0815
4	30	1	3	12,0636	21,629	12,8423
4	30	5	7	7,6988	17,728	6,8391
4	60	0,2	0	28,2897	29,032	28,2397
4	60	1	3	21,0526	26,466	25,0005
4	60	5	7	15,7898	23,967	18,9973
4	90	0,2	3	43,9402	32,857	39,2640
4	90	1	7	33,4721	30,493	36,0903
4	90	5	0	22,3150	26,971	17,2394
10	30	0,2	7	18,2073	25,204	24,1389
10	30	1	0	11,3136	21,072	8,1176
10	30	5	3	4,8128	13,647	2,0489
10	60	0,2	3	32,0930	30,128	31,9927
10	60	1	7	38,5021	31,709	28,8190
10	60	5	0	7,2901	17,254	9,9682
10	90	0,2	7	44,2969	32,927	43,0825
10	90	1	0	21,5269	26,659	27,0612
10	90	5	3	18,1788	25,191	20,9925

4. CONCLUSION

As it is known, water pollution poses a great threat to the survival of life. With the development of technology, developing industrial sectors mix serious wastewater into clean water resources. This situation affects the health of living beings with diseases that can be fatal. Various traditional methods are used for water purification, but these methods are not efficient at the nanoparticle level and create secondary pollution. For this reason, the tendency towards new generation methods has increased recently. Methods emerging from nanotechnology are among the most frequently researched technologies in this field. Photocatalysis, which is an advanced oxidative process method, is one of these methods. Photocatalysis consists of a series of reactions that enable the elimination of organic materials with the help of reduction-oxidation reactions in the presence of light. Light and photocatalyst are required for photocatalysis. Photocatalysts create electron-hole pairs with the energy they receive from light, allowing electrons to move from the valence band to the conduction band, and with this initial move, reduction and oxidation reactions are enabled. As a result of these reactions, unstable hydroxyl and oxygen anion radicals are formed, polluting materials are eliminated and the reactions end with the formation of carbon dioxide and water. In this study, it was aimed to improve the photocatalytic and electrical properties of ZnO nanorods, which are metal oxide semiconductors, by doping boron using the hydrothermal method. Then, the optimum conditions were determined with the minimum number of experiments for the photocatalyst obtained, and the best conditions among the pH, time, concentration and dope amount factors were determined by the Taguchi method, one of the design of experiment methods. As a result of the experiments, pure and boron-doped samples (1, 3, 5, 7, 10 wt%) were successfully synthesized. The synthesized samples were characterized with the help of XRD, FT-IR, SEM, UV-Vis devices. It was kept in methylene blue, an organic dye, under UV-A light in a closed environment, at different pH (4, 7, 10) and methylene blue concentrations ($2x10^{-6}$ M, $1x10^{-5}$ M, $5x10^{-5}$ M) for 90 minutes for

photodegradation. According to the results obtained, the synthesized samples grew in the (002) c orientation. With the increase in boron doped, there was also a proportional growth in the (100) orientation. Due to the low atomic radius of the boron element, a shift in the peak angle towards the low angle is expected to indicate that it has been successfully incorporated into the crystal structure. XRD results showed us this shift and gave us an idea that boron addition was successful. The particle sizes obtained as a result of XRD analysis also showed that they were compatible with SEM. According to the subsequent FT-IR analysis, peak formation in the range of 1300-1700 cm^{-1}, where B-O and B-O-B peaks are located, was observed with the increase of boron contribution. As a result of the analyzes performed with the UV-Vis spectrometer, it was seen that boron-doped samples provided absorbance in the visible light region compared to pure ZnO nanorods, giving an idea that the band gap decreased in this case. This situation was confirmed by the band gap calculated according to UV-Vis results. As a result of band gap calculations, pure ZnO nanorods have a band gap of 3.22 eV, while boron doped ones have a lower band gap. ZnO nanorods with 3% boron doping have the lowest band gap with a value of 2.97 eV. As a result of the temperature-dependent AC-DC electrical analyses, it was seen that the conductivity increased with the increase of boron doped, and the samples that exhibited a semiconductor behavior turned into a metallic behavior as the boron contribution increased. It is thought that as the conductivity increases, the conduction band and valence band gap decreases, boron doping gives electrons to the medium and increases electrical conduction by establishing electron traps in the band gap. Finally, photocatalytic tests have shown that photocatalytic efficiency increases with increasing boron contribution. For $2x10^{-6}$ M concentration, 3% B-doped ZnO nanorods showed the best results with a rate constant of 0.00856 min^{-1}. For $1x10^{-5}$ M concentration, 7% B-doped ZnO nanorods showed the best results with a rate constant value of 0.00665 min^{-1}. Finally, for $5x10^{-5}$ M concentration, the 3% doped sample showed the best result with a rate constant value of 0.00308 min^{-1}. When we compare the numerical values of the rate constants, under the same conditions, the 1% B doped sample has a 94% higher rate than the pure ZnO sample for pH 4. For pH 7, the 3% B-doped sample has a 36% higher rate than pure ZnO, and finally for pH 10, the 7% B-doped sample has a 194% higher rate constant. It has been proven that the band gap decreases with the increase in conductivity with the boron doped, photocatalytic efficiency increases with the effects of electron pumping by boron gaining electrons

lost with oxygen in the crystal structure, increasing homogeneous surface area, and the possibility of recombination decreases with the increase in surface defects and photostability improves. Finally, the optimum conditions were determined among pH, concentration, time and additive amount by the Taguchi method applied to determine the optimum conditions with the minimum number of experiments. In this case, it has been observed that our photocatalyst works best in the pH range of 4, at a concentration of $2x10^{-6}$ M, for 90 minutes, with 7% boron contribution. Here, pH affects the surface state of the catalyst and the ionization state of ionizable organic compounds, thereby affecting the interfacial electron transfer and photoredox process. Additionally, depending on pH, hydroxyl radical production plays an important role in reaction mechanisms that can contribute to pollutant degradation, such as direct oxidation by the positive hole and direct reduction by the electron in the conduction band. As the time factor increases up to a point, the photocatalytic efficiency increases, but when it reaches the saturation point, the efficiency remains constant. In this study, the time was determined as 90 minutes. Another parameter is concentration. By adjusting the concentration amount, we can increase or decrease the amount of adhesion of pollutants to the surfaces, and the penetration of light can also be changed by concentration. Finally, the effect of the doped amount was examined. As the amount of doped increases up to a certain level, surface defects increase, conductivity increases, surface area increases and photocatalytic efficiency increases. Thus, it was shown that 7% doped amount was the most suitable for this study. The compatibility of the model was determined via ANOVA and R^2 showed a good fit of 85%. As a result of this study, it has been proven that boron doped increases the photocatalytic efficiency and electrical conductivity by 5 times for DC and 3 times for AC. It has been shown that boron additive has the potential to be developed for ZnO in areas such as photocatalyst, pollutant treatment, hydrogen storage and sensors.

REFERANCES

[1] **Feynman, R. P.** (1992). There's plenty of room at the bottom [data storage]. Journal of microelectromechanical systems, 1(1), 60-66.

[2] **Ukaogo, P. O., Ewuzie, U., & Onwuka, C. V.** (2020). Environmental pollution: causes, effects, and the remedies. In Microorganisms for sustainable environment and health (pp. 419-429). Elsevier.

[3] **Landrigan, P. J., Fuller, R., Acosta, N. J., Adeyi, O., Arnold, R., Baldé, A. B., ... & Zhong, M.** (2018). The Lancet Commission on pollution and health. The lancet, 391(10119), 462-512.

[4] **Perera, F. P.** (2017). Multiple threats to child health from fossil fuel combustion: impacts of air pollution and climate change. Environmental health perspectives, 125(2), 141-148.

[5] **Landrigan, P. J., & Fuller,** (2012). Environmental pollution: an enormous and invisible burden on health systems in low-and middle-income counties. World Hosp Health Serv, 50(4), 35..

[6] **Haseena, M., Malik, M. F., Javed, A., Arshad, S., Asif, N., Zulfiqar, S., & Hanif, J.** (2017). Water pollution and human health. Environmental Risk Assessment and Remediation, 1(3).

[7] **Briggs, D.** (2003). Environmental pollution and the global burden of disease. British medical bulletin, 68(1), 1-24.

[8] **World Health Organization,** 2023. Available: https://www.who.int/en/news-room/fact-sheets/detail/drinking-water.

[9] **Ewuzie, U., Nnorom, I. C., & Eze, S. O.** (2020). Lithium in drinking water sources in rural and urban communities in Southeastern Nigeria. Chemosphere, 245, 125593.

[10] **Kamble, S. M.** (2014). Water pollution and public health issues in Kolhapur city in Maharashtra. International journal of scientific and research publications, 4(1), 1-6.

[11] **Desai, N.** (2014). SmtVanitaben. A study on the water pollution based on the environmental problem. Indian Journal of Research, 3(12), 95-96.

[12] **Al-Tohamy, R., Ali, S. S., Li, F., Okasha, K. M., Mahmoud, Y. A. G., Elsamahy, T., ... & Sun, J.** (2022). A critical review on the treatment of dye-containing wastewater: Ecotoxicological and health concerns of textile dyes and possible remediation approaches for environmental safety. Ecotoxicology and Environmental Safety, 231, 113160.

[13] **Jin, X. C., Liu, G. Q., Xu, Z. H., & Tao, W. Y.** (2007). Decolorization of a dye industry effluent by Aspergillus fumigatus XC6. Applied microbiology and biotechnology, 74, 239-243.

[14] **Ministry of Health, Water Safety Plan Guide:** Treatment Processes – Conventional Coagulation/Flocculation/Sedimentation, Version 1, Ref P5.1., Wellington: Ministry of Health PO Box 5013, 2014.

[15] **Hairom, N. H. H., Soon, C. F., Mohamed, R. M. S. R., Morsin, M., Zainal, N., Nayan, N., ... & Harun, N. H.** (2021). A review of nanotechnological applications to detect and control surface water pollution. Environmental Technology & Innovation, 24, 102032.

[16] **Liew, W. L., Kassim, M. A., Muda, K., Loh, S. K., & Affam, A. C.** (2015). Conventional methods and emerging wastewater polishing technologies for palm oil mill effluent treatment: a review. Journal of environmental management, 149, 222-235.

[17] **Maurya, A., Singh, M. K., & Kumar, S.** (2020). Biofiltration technique for removal of waterborne pathogens. In Waterborne pathogens (pp. 123-141). Butterworth-Heinemann.

[18] **Bhushan, B.** (2017). Introduction to nanotechnology. Springer handbook of nanotechnology, 1-19.

[19] **Bhushan, B., Luo, D., Schricker, S. R., Sigmund, W., & Zauscher, S. (Eds.).** (2014). Handbook of nanomaterials properties. Springer Science & Business Media.

[20] **Bhushan, B.** (2015). Governance, policy, and legislation of nanotechnology: a perspective. Microsystem Technologies, 21, 1137-1155.

[21] **Theron, J., Walker, J. A., & Cloete, T. E.** (2008). Nanotechnology and water treatment: applications and emerging opportunities. *Critical reviews in microbiology*, *34*(1), 43-69.

[22] **Qu, X., Alvarez, P. J., & Li, Q.** (2013). Applications of nanotechnology in water and wastewater treatment. Water research, 47(12), 3931-3946.

[23] **Baruah, S., Najam Khan, M., & Dutta, J.** (2016). Perspectives and applications of nanotechnology in water treatment. Environmental chemistry letters, 14, 1-14.

[24] **Baruah, S., Jaisai, M., & Dutta, J.** (2012). Development of a visible light active photocatalytic portable water purification unit using ZnO nanorods. Catalysis Science & Technology, 2(5), 918-921.

[25] **Pelizzetti P.** (1989) Photocatalysis: Fundamentals and Applications, New York, 1989.

[26] **Plotnikow J.** (1910) Textbook of Photochemistry, Berlin: Verlag von Willhelm Knapp, 1910.

[27] **Baly, E. C. C., Heilbron, I. M., & Barker, W. F.** (1921). CX.—Photocatalysis. Part I. The synthesis of formaldehyde and carbohydrates from carbon dioxide and water. Journal of the Chemical Society, Transactions, 119, 1025-1035.

[28] **Fujishima, A., & Honda, K.** (1972). Electrochemical photolysis of water at a semiconductor electrode. nature, 238(5358), 37-38..

[29] **Inoue, T., Fujishima, A., Konishi, S., & Honda, K.** (1979). Photoelectrocatalytic reduction of carbon dioxide in aqueous suspensions of semiconductor powders. Nature, 277(5698), 637-638.

[30] **Sordello, F., Calza, P., Minero, C., Malato, S., & Minella, M.** (2022). More than one century of history for photocatalysis, from past, present and future perspectives. Catalysts, 12(12), 1572.

[31] **Yang, X., & Wang, D.** (2018). Photocatalysis: from fundamental principles to materials and applications. *ACS Applied Energy Materials*, *1*(12), 6657-6693.

[32] **Wang, L., & Yu, J.** (2023). Principles of photocatalysis. In *Interface Science and Technology* (Vol. 35, pp. 1-52). Elsevier.

[33] **Zhu, S., & Wang, D.** (2017). Photocatalysis: basic principles, diverse forms of implementations and emerging scientific opportunities. *Advanced Energy Materials*, *7*(23), 1700841.

[34] **Mamaghani, A. H., Haghighat, F., & Lee, C. S.** (2017). Photocatalytic oxidation technology for indoor environment air purification: The state-of-the-art. *Applied Catalysis B: Environmental*, *203*, 247-269..

[35] **Khan, M. M., Pradhan, D., & Sohn, Y. (Eds.).** (2017). *Nanocomposites for visible light-induced photocatalysis* (Vol. 101). Cham, Switzerland: Springer International Publishing..

[36] **Gautam, S., Agrawal, H., Thakur, M., Akbari, A., Sharda, H., Kaur, R., & Amini, M.** (2020). Metal oxides and metal organic frameworks for the photocatalytic degradation: A review. *Journal of Environmental Chemical Engineering*, *8*(3), 103726.

[37] **Kiriakidis, G., & Binas, V.** (2014). Metal oxide semiconductors as visible light photocatalysts. *Journal of the Korean Physical Society*, *65*, 297-302.

[38] **Rodriguez, J. A., & Fernández-García, M. (Eds.).** (2007). *Synthesis, properties, and applications of oxide nanomaterials*. John Wiley & Sons..

[39] **Theerthagiri, J., Chandrasekaran, S., Salla, S., Elakkiya, V., Senthil, R. A., Nithyadharseni, P., ... & Kim, H. S.** (2018). Recent developments of metal oxide based heterostructures for photocatalytic applications towards environmental remediation. *Journal of Solid State Chemistry*, *267*, 35-52.

[40] **Gusain, R., Gupta, K., Joshi, P., & Khatri, O. P.** (2019). Adsorptive removal and photocatalytic degradation of organic pollutants using metal oxides and their composites: A comprehensive review. *Advances in colloid and interface science*, *272*, 102009.

[41] **Meshram, S. P., Adhyapak, P. V., Mulik, U. P., & Amalnerkar, D. P.** (2012). Facile synthesis of CuO nanomorphs and their morphology dependent sunlight driven photocatalytic properties. *Chemical engineering journal*, *204*, 158-168.

[42] **Kar, A., Olszówka, J., Sain, S., Sloman, S. R. I., Montes, O., Fernández, A., ... & Wheatley, A. E.** (2019). Morphological effects on the

photocatalytic properties of SnO2 nanostructures. *Journal of Alloys and Compounds*, *810*, 151718

[43] **Wang, C., Shao, C., Wang, L., Zhang, L., Li, X., & Liu, Y.** (2009). Electrospinning preparation, characterization and photocatalytic properties of Bi2O3 nanofibers. *Journal of colloid and interface science*, *333*(1), 242-248

[44] **Shandilya, P., Sambyal, S., Sharma, R., Mandyal, P., & Fang, B.** (2022). Properties, optimized morphologies, and advanced strategies for photocatalytic applications of WO3 based photocatalysts. *Journal of Hazardous Materials*, *428*, 128218.

[45] **Ramesh, M., Rao, M. P. C., Anandan, S., & Nagaraja, H.** (2018). Adsorption and photocatalytic properties of NiO nanoparticles synthesized via a thermal decomposition process. *Journal of Materials Research*, *33*(5), 601-610.

[46] **Danish, M. S. S., Estrella, L. L., Alemaida, I. M. A., Lisin, A., Moiseev, N., Ahmadi, M., ... & Senjyu, T.** (2021). Photocatalytic applications of metal oxides for sustainable environmental remediation. *Metals*, *11*(1), 80.

[47] **Wang, Z. L.** (2004). Zinc oxide nanostructures: growth, properties and applications. *Journal of physics: condensed matter*, *16*(25), R829

[48] **A Barzinjy, A.** (2021). Synthesis, properties and uses of ZnO nanorods: a mini review. *International Nano Letters*.

[49] **Willander, M., Nur, O., Zhao, Q. X., Yang, L. L., Lorenz, M., Cao, B. Q., ... & Dang, D. L. S.** (2009). Zinc oxide nanorod based photonic devices: recent progress in growth, light emitting diodes and lasers. *Nanotechnology*, *20*(33), 332001.

[50] **Öztürk, S., Kılınç, N., & Öztürk, Z. Z.** (2013). Fabrication of ZnO nanorods for NO2 sensor applications: effect of dimensions and electrode position. *Journal of Alloys and Compounds*, *581*, 196-201.

[51] **Lee, K. M., Lai, C. W., Ngai, K. S., & Juan, J. C.** (2016). Recent developments of zinc oxide based photocatalyst in water treatment technology: a review. *Water research*, *88*, 428-448.

[52] **Mehrabian, M., Azimirad, R., Mirabbaszadeh, K., Afarideh, H., & Davoudian, M.** (2011). UV detecting properties of hydrothermal synthesized ZnO nanorods. *Physica E: Low-dimensional Systems and Nanostructures*, *43*(6), 1141-1145.

[53] **Klingshirn, C.** (2007). ZnO: material, physics and applications. *ChemPhysChem*, *8*(6), 782-803.

[54] **Maggard, P. A., Stern, C. L., & Poeppelmeier, K. R.** (2001). Understanding the role of helical chains in the formation of noncentrosymmetric solids. *Journal of the American Chemical Society*, *123*(31), 7742-7743.

[55] **Banerjee, D., Lao, J. Y., Wang, D. Z., Huang, J. Y., Ren, Z. F., Steeves, D., ... & Sennett, M.** (2003). Large-quantity free-standing ZnO nanowires. Applied Physics Letters, 83(10), 2061-2063.

[56] **Kong, X. Y., Ding, Y., Yang, R., & Wang, Z. L.** (2004). Single-crystal nanorings formed by epitaxial self-coiling of polar nanobelts. Science, 303(5662), 1348-1351.

[57] **Wahab, R., Ansari, S. G., Kim, Y. S., Seo, H. K., & Shin, H. S.** (2007). Room temperature synthesis of needle-shaped ZnO nanorods via sonochemical method. *Applied Surface Science*, *253*(18), 7622-7626.

[58] **Chiu, W. S., Khiew, P. S., Cloke, M., Isa, D., Tan, T. K., Radiman, S., ... & Chia, C. H.** (2010). Photocatalytic study of two-dimensional ZnO nanopellets in the decomposition of methylene blue. *Chemical Engineering Journal*, *158*(2), 345-352.

[59] **Xie, Q., Dai, Z., Liang, J., Xu, L., Yu, W., & Qian, Y.** (2005). Synthesis of ZnO three-dimensional architectures and their optical properties. *Solid state communications*, *136*(5), 304-307.

[60] **Pearton, S. J., Norton, D. P., Ip, K., Heo, Y. W., & Steiner, T.** (2003). Recent progress in processing and properties of ZnO. Superlattices and Microstructures, 34(1-2), 3-32.

[61] **Abdullah, F. H., Bakar, N. A., & Bakar, M. A.** (2022). Current advancements on the fabrication, modification, and industrial application of zinc oxide as photocatalyst in the removal of organic and inorganic contaminants in aquatic systems. *Journal of hazardous materials*, *424*, 127416.

[62] **Curri, M. L., Comparelli, R., Cozzoli, P. D., Mascolo, G., & Agostiano, A.** (2003). Colloidal oxide nanoparticles for the photocatalytic degradation of organic dye. *Materials Science and Engineering: C*, *23*(1-2), 285-289.

[63] **Singh, T. A., Das, J., & Sil, P. C.** (2020). Zinc oxide nanoparticles: A comprehensive review on its synthesis, anticancer and drug delivery applications as well as health risks. *Advances in colloid and interface science*, *286*, 102317.

[64] **Noman, M. T., Amor, N., & Petru, M.** (2022). Synthesis and applications of ZnO nanostructures (ZONSs): A review. *Critical Reviews in Solid State and Materials Sciences*, *47*(2), 99-141.

[65] **Benhebal, H., Chaib, M., Salmon, T., Geens, J., Leonard, A., Lambert, S. D., ... & Heinrichs, B.** (2013). Photocatalytic degradation of phenol and benzoic acid using zinc oxide powders prepared by the sol–gel process. *Alexandria Engineering Journal*, *52*(3), 517-523.

[66] **Hasnidawani, J. N., Azlina, H. N., Norita, H., Bonnia, N. N., Ratim, S., & Ali, E. S.** (2016). Synthesis of ZnO nanostructures using sol-gel method. *Procedia Chemistry*, *19*, 211-216.

[67] **Saravanan, R., Thirumal, E., Gupta, V. K., Narayanan, V., & Stephen, A.** (2013). The photocatalytic activity of ZnO prepared by simple thermal decomposition method at various temperatures. *Journal of Molecular Liquids*, *177*, 394-401.

[68] **Zhang, Y., Ram, M. K., Stefanakos, E. K., & Goswami, D. Y.** (2012). Synthesis, characterization, and applications of ZnO nanowires. *Journal of Nanomaterials*, *2012*, 1-22.

[69] **Kumaresan, N., Ramamurthi, K., Babu, R. R., Sethuraman, K., & Babu, S. M.** (2017). Hydrothermally grown ZnO nanoparticles for effective photocatalytic activity. *Applied Surface Science*, *418*, 138-146.

[70] **Agarwal, S., Rai, P., Gatell, E. N., Llobet, E., Güell, F., Kumar, M., & Awasthi, K.** (2019). Gas sensing properties of ZnO nanostructures (flowers/rods) synthesized by hydrothermal method. *Sensors and Actuators B: Chemical*, *292*, 24-31.

[71] **Chen, L., Batjikh, I., Hurh, J., Han, Y., Huo, Y., Ali, H., ... & Yang, D. C.** (2019). Green synthesis of zinc oxide nanoparticles from root extract of Scutellaria baicalensis and its photocatalytic degradation activity using methylene blue. *Optik*, *184*, 324-329.

[72] **Adam, R. E., Pozina, G., Willander, M., & Nur, O.** (2018). Synthesis of ZnO nanoparticles by co-precipitation method for solar driven photodegradation of Congo red dye at different pH. *Photonics and Nanostructures-Fundamentals and Applications*, *32*, 11-18.

[73] **Chen, Y. C., & Lo, S. L.** (2011). Effects of operational conditions of microwave-assisted synthesis on morphology and photocatalytic capability of zinc oxide. *Chemical Engineering Journal*, *170*(2-3), 411-418.

[74] **Jassby, D., Farner Budarz, J., & Wiesner, M.** (2012). Impact of aggregate size and structure on the photocatalytic properties of TiO2 and ZnO nanoparticles. *Environmental science & technology*, *46*(13), 6934-6941.

[75] **Sushma, C., & Girish Kumar, S.** (2017). Advancements in the zinc oxide nanomaterials for efficient photocatalysis. *Chemical Papers*, *71*(10), 2023-2042.

[76] **Samadi, M., Zirak, M., Naseri, A., Kheirabadi, M., Ebrahimi, M., & Moshfegh, A. Z.** (2019). Design and tailoring of one-dimensional ZnO nanomaterials for photocatalytic degradation of organic dyes: a review. *Research on Chemical Intermediates*, *45*, 2197-2254.

[77] **Gerischer, H.** (1966). Electrochemical behavior of semiconductors under illumination. *Journal of the electrochemical society*, *113*(11), 1174.

[78] **Das, A., Nikhil, S. K., & Nair, R. G.** (2019). Influence of surface morphology on photocatalytic performance of zinc oxide: A review. *Nano-Structures & Nano-Objects*, *19*, 100353.

[79] **Zhang, X., Qin, J., Xue, Y., Yu, P., Zhang, B., Wang, L., & Liu, R.** (2014). Effect of aspect ratio and surface defects on the photocatalytic activity of ZnO nanorods. *Scientific reports*, *4*(1), 4596.

[80] **D Kaneva, N. V., Dimitrov, D. T., & Dushkin, C. D.** (2011). Effect of nickel doping on the photocatalytic activity of ZnO thin films under UV and visible light. *Applied Surface Science*, *257*(18), 8113-8120.

[81] **Adam, R. E., Alnoor, H., Pozina, G., Liu, X., Willander, M., & Nur, O.** (2020). Synthesis of Mg-doped ZnO NPs via a chemical low-temperature method and investigation of the efficient

photocatalytic activity for the degradation of dyes under solar light. *Solid State Sciences*, *99*, 106053.

[82] **Al Abri, R., Al Marzouqi, F., Kuvarega, A. T., Meetani, M. A., Al Kindy, S. M., Karthikeyan, S., ... & Selvaraj, R.** (2019). Nanostructured cerium-doped ZnO for photocatalytic degradation of pharmaceuticals in aqueous solution. *Journal of Photochemistry and Photobiology A: Chemistry*, *384*, 112065.

[83] **Qi, K., Xing, X., Zada, A., Li, M., Wang, Q., Liu, S. Y., ... & Wang, G.** (2020). Transition metal doped ZnO nanoparticles with enhanced photocatalytic and antibacterial performances: experimental and DFT studies. *Ceramics International*, *46*(2), 1494-1502.

[84] **Di Valentin, C., & Pacchioni, G.** (2013). Trends in non-metal doping of anatase TiO2: B, C, N and F. *Catalysis today*, *206*, 12-18.

[85] **Tang, C., Chen, C., Zhang, H., Zhang, J., & Li, Z.** (2020). Enhancement of degradation for nitrogen doped zinc oxide to degrade methylene blue. *Physica B: Condensed Matter*, *583*, 412029.

[86] **Ramalingam, R. J., Shukla, A. K., Kombaiah, K., Vijaya, J. J., & Tawfeek, A. M.** (2017). Synthesis, characterization and optical properties of sulfur and fluorine doped ZnO nanostructures for visible light utilized catalysis. *Optik*, *148*, 325-331.

[87] **Mardikar, S. P., Kulkarni, S., & Adhyapak, P. V.** (2020). Sunlight driven highly efficient degradation of methylene blue by CuO-ZnO nanoflowers. *Journal of Environmental Chemical Engineering*, *8*(2), 102788.

[88] **Mugunthan, E., Saidutta, M. B., & Jagadeeshbabu, P. E.** (2019). Photocatalytic activity of ZnO-WO3 for diclofenac degradation under visible light irradiation. *Journal of Photochemistry and Photobiology A: Chemistry*, *383*, 111993.

[89] **Shan, A. Y., Ghazi, T. I. M., & Rashid, S. A.** (2010). Immobilisation of titanium dioxide onto supporting materials in heterogeneous photocatalysis: A review. *Applied Catalysis A: General*, *389*(1-2), 1-8.

[90] **Chong, M. N., Jin, B., Chow, C. W., & Saint, C.** (2010). Recent developments in photocatalytic water treatment technology: a review. *Water research*, *44*(10), 2997-3027.

[91] **Debroye, E., Van Loon, J., Yuan, H., Janssen, K. P., Lou, Z., Kim, S., ... & Roeffaers, M. B.** (2017). Facet-dependent photoreduction on single ZnO crystals. *The journal of physical chemistry letters*, *8*(2), 340-346.

[92] **Zhong, J. B., Li, J. Z., He, X. Y., Zeng, J., Lu, Y., He, J. J., & Zhong, F.** (2014). Fabrication and catalytic performance of SiO2-ZnO composite photocatalyst. *Synthesis and Reactivity in Inorganic, Metal-Organic, and Nano-Metal Chemistry*, *44*(8), 1203-1207.

[93] **Iqbal, A., Saidu, U., Adam, F., Sreekantan, S., Yahaya, N., Ahmad, M. N., ... & Wilson, L. D.** (2021). Floating ZnO QDs-modified TiO2/LLDPE hybrid polymer film for the effective

photodegradation of tetracycline under fluorescent light irradiation: Synthesis and characterisation. *Molecules*, *26*(9), 2509.

[94] **Shah, A. P., Jain, S., Mokale, V. J., & Shimpi, N. G.** (2019). High performance visible light photocatalysis of electrospun PAN/ZnO hybrid nanofibers. *Journal of Industrial and Engineering Chemistry*, *77*, 154-163.

[95] **Massaro, M., Casiello, M., D'Accolti, L., Lazzara, G., Nacci, A., Nicotra, G., ... & Riela, S.** (2020). One-pot synthesis of ZnO nanoparticles supported on halloysite nanotubes for catalytic applications. *Applied Clay Science*, *189*, 105527.

[96] **Akkari, M., Aranda, P., Belver, C., Bedia, J., Amara, A. B. H., & Ruiz-Hitzky, E.** (2018). Reprint of ZnO/sepiolite heterostructured materials for solar photocatalytic degradation of pharmaceuticals in wastewater. *Applied Clay Science*, *160*, 3-8.

[97] **Furka, D., Furka, S., Naftaly, M., Rakovský, E., Čaplovičová, M., & Janek, M.** (2021). ZnO nanoparticles as photodegradation agent controlled by morphology and boron doping. *Catalysis Science & Technology*, *11*(6), 2167-2185.

[98] **Senol, S. D., Ozturk, O., & Terzioğlu, C.** (2015). Effect of boron doping on the structural, optical and electrical properties of ZnO nanoparticles produced by the hydrothermal method. *Ceramics International*, *41*(9), 11194-11201.

[99] **Núñez-Salas, R. E., Hernández-Ramírez, A., Hinojosa-Reyes, L., Guzmán-Mar, J. L., Villanueva-Rodriguez, M., & de Lourdes Maya-Trevino, M.** (2019). Cyanide degradation in aqueous solution by heterogeneous photocatalysis using boron-doped zinc oxide. *Catalysis Today*, *328*, 202-209.

[100] **Atay, & Gultepe, O.** (2022). Structural, optical and surface properties of sol–gel-derived boron-doped ZnO films for photocatalytic applications. *Applied Physics A*, *128*, 1-13..

[101] **Z Kayani, Z. N., Bashir, Z., Riaz, S., Naseem, S., & Saddiqe, Z.** (2020). Transparent boron-doped zinc oxide films for antibacterial and magnetic applications. *Journal of Materials Science: Materials in Electronics*, *31*, 11911-11926.

[102] **Wang, W., Ai, T., & Yu, Q.** (2017). Electrical and photocatalytic properties of boron-doped ZnO nanostructure grown on PET–ITO flexible substrates by hydrothermal method. *Scientific reports*, *7*(1), 42615.

[103] **Sharma, A., Chakraborty, M., Thangavel, R., & Udayabhanu, G.** (2018). Hydrothermal growth of undoped and boron doped ZnO nanorods as a photoelectrode for solar water splitting applications. *Journal of Sol-Gel Science and Technology*, *85*, 1-11.

[104] **Şahin, Y., Öztürk, S., Kılınc, N., Kösemen, A., Erkovan, M., & Öztürk, Z. Z.** (2014). Electrical conduction and NO2 gas sensing properties of ZnO nanorods. *Applied Surface Science*, *303*, 90-96.

[105] **Öztürk, S., Kılınç, N., Taşaltın, N., & Öztürk, Z. Z.** (2012). Fabrication of ZnO nanowires and nanorods. *Physica E: Low-Dimensional Systems and Nanostructures*, *44*(6), 1062-1065.

[106] **Gultepe, O., Atay & Dikmen,** (2023). An effective approach for hydrothermal synthesis of ZnO nanorod arrays activated under UV/Vis light: Different supporting ligands for hydrothermal precursor solutions. *Materials Chemistry and Physics*, *307*, 128170.

[107] **Davis, R., & John, P.** (2018). Application of Taguchi-based design of experiments for industrial chemical processes. *Statistical approaches with emphasis on design of experiments applied to chemical processes*, *137*.

[108] **Caglar, Y., Ilican, S., & Caglar, M.** (2017). FESEM, XRD and DRS studies of electrochemically deposited boron doped ZnO films. *Materials Science-Poland*, *35*(4), 824-829.

[109] **Senol, S. D., Ozugurlu, E., & Arda, L.** (2020). The effect of cobalt and boron on the structural, microstructural, and optoelectronic properties of ZnO nanoparticles. *Ceramics International*, *46*(6), 7033-7044.

[110] **Kılınç, N., Arda, L., Öztürk, S., & Öztürk, Z. Z.** (2010). Structure and electrical properties of Mg-doped ZnO nanoparticles. *Crystal Research and Technology*, *45*(5), 529-538.

[111] **Şahin, Y., Öztürk, S., Kılınc, N., Kösemen, A., Erkovan, M., & Öztürk, Z. Z.** (2014). Electrical conduction and NO2 gas sensing properties of ZnO nanorods. *Applied Surface Science*, *303*, 90-96.

[112] **Alkaim, A. F., Aljeboree, A. M., Alrazaq, N. A., Baqir, S. J., Hussein, F. H., & Lilo, A. J.** (2014). Effect of pH on adsorption and photocatalytic degradation efficiency of different catalysts on removal of methylene blue. *Asian Journal of Chemistry*, *26*(24), 8445.

[113] **Yu, Q., Jiang, L., Gao, S., Zhang, S., Ai, T., Feng, X., & Wang, W.** (2017). The highly efficient photocatalysts of B-doped ZnO microspheres synthesized on PET-ITO flexible substrate. *Ceramics International*, *43*(2), 2864-2866.

CIRRICULUM VITAE

Name Surname: Eray TABAK

EDUCATION:

B.Sc. : 2020, Yildiz Technical University, Faculty of Chemical and Metallurgical Engineering, Bioengineering

PROFESSIONAL EXPERIENCE AND PUBLICATIONS:

- Tasci, M. E., Dede, B., Tabak, E., Gur, A., Sulutas, R. B., Cesur, S., ... & Gunduz, O. (2021). Production, optimization and characterization of polylactic acid microparticles using electrospray with porous structure. Applied Sciences, 11(11), 5090

- TUBITAK-2210-C Domestic Graduate Scholarship Programme for Priority Areas.

PUBLICATIONS, PRESENTATIONS AND PATENTS ON THE THESIS:

- Eray Tabak, Production of boron and nanoclay doped zinc oxide nanorods and compared their properties and improvement of their photocatalytic properties, International Graduate Research Symposium, Istanbul, 2023